Master's thesis

NTNU
Norwegian University of Science and Technology
Faculty of Information Technology and Electrical Engineering
Department of Electronic Systems

Einar Avdem

Long-Range Low Frequency (LF) Radio Frequency Identification (RFID)

For detecting individual animals identity in wearable Internet of Things (IoT) devices

Master's thesis in Electronic Systems Design
Supervisor: Egil Eide
June 2022

NTNU
Norwegian University of Science and Technology

Einar Avdem

Long-Range Low Frequency (LF) Radio Frequency Identification (RFID)

For detecting individual animals identity in wearable Internet of Things (IoT) devices

Master's thesis in Electronic Systems Design
Supervisor: Egil Eide
June 2022

Norwegian University of Science and Technology
Faculty of Information Technology and Electrical Engineering
Department of Electronic Systems

NTNU
Norwegian University of
Science and Technology

Preface

This report is the end result of the course *TFE4930 - Electronic Systems Design, Master's Thesis*, and was done during the final semester of the two-years Master's degree programme *Electronic Systems Design* at Norwegian University of Science and Technology (NTNU), under the Analog Circuit Design and Radio Systems specialization option. The project is given by Nofence AS as a study project for gaining technical insight on Radio Frequency Identification (RFID) used on livestock in agriculture.

Acknowledgements

Foremost I would like to thank my supervisor Egil Eide for guidance and good discussions, that helped defined the scope and direction of this project. I would also like to thank Oscar Berntsen and the rest of the staff at Nofence for granting this unique project.

Additionally, I would like to thank Ståle Berre & Pål Dalløkken at OSID for supplying both kinds of RFID transponders that are in use with livestock identification. I would also like to thank Irene Jensen at SINTEF for letting me borrow the measurement antenna and Terje Mathisen for help sourcing equipment for testing.

I would also like to thank my fellow students Edvard Birkeland and Thomas Bolle sharing their insight with the C programming language, and helping with it.

Finally, I would like to express my gratitude for being allowed to attend the Analog Circuit Design and Radio Systems specialization over the past two years. As these are in my eyes some of the most interesting concepts that I know of. I am very thankful that what interests me the most is something available to study, and that I have over the past years been allowed to learn from some really skilled people with a high degree of knowledge and theoretical insight within these concepts. Not only have I learned some of the key elements within the specialization, but I have learned how to go about learning new things, which I am sure will help me throughout the rest of my life.

Einar Avdem
Trondheim, 13th June 2022

Abstract

Internet of Things (IoT) in agriculture is an increasingly growing market. IoT products in this industry are usually aimed at farming animals, where normal use cases can be: tracking animal movement, sleep tracking, and monitoring food intake to name a few.

Nofence AS produces Global Navigation Satellite Systems (GNSS) based collars which are used for geofencing for farming animals. A concern with these products is the linking of device identity with the individual animal's identity, essentially: which animal is wearing which device?

A possible solution can be using Low Frequency (LF) Radio Frequency Identification (RFID) ear tags that are already mandatory for farming animals in many countries.

This thesis describes the implementation of two long-range LF RFID prototype systems to research possible configurations that can be used for Nofences products. Two systems are implemented to work for each of the protocols that are used for LF RFID for farming animals.

The implementation includes the design of two circuits that are based on two Application Specific Integrated Circuits (ASICs), one for each protocol. The systems are verified with two types of measurements. Firstly the interrogation zone, which is the zone where the reader can detect a transponder, of each system is measured using two transponder angles. Secondly, the transmitted magnetic field strength of each reader is measured to verify that the system does not violate ETSI regulations and to give further insight into the system's performance.

Both systems can achieve greater distance reading than close proximity, 30 cm for the HDX system and 15 cm for the FDX-B system, while maintaining very limited physical dimensions. This is done by using ferrite core antennas.

1 Sammendrag

Det er et økende marked for Internet of Things (IoT), innen landbruket. IoT produkter i denne industrien er ofte rettet mot husdyr, hvor vanlige bruksområder kan være: kartlegging av dyrenes bevegelser, kartlegging av søvn og kartlegging av matinntak for å nevne noen.

Nofence AS produserer Global Navigation Satellite Systems (GNSS)-baserte klaver som muliggjør virituelle gjerder for husdyr. Det er en utfordring med disse produktene å sikre koblingen mellom klavens identitet, og hvert individs identitet - altså hvilket husdyr bruker hvilken klave?

En mulig løsning for dette problemet er å lese Lav Frekvent (LF) Radiofrekvensidentifikasjon (RFID) øremerker som allerede er lovpålagt husdyr i mange land, for å knytte klavens identitet med individets identitet.

Denne oppgaven beskriver implementasjonen av to langdistanse LF RFID leser prototyper, for å undersøke mulige konfigurasjoner Nofence kan bruke i sine produkter. To systemer er implementert, et for hver protokoll som benyttes i LF RFID for husdyr.

Implementasjonen består av designet av to kretser som baserer seg på to Applikasjonsspesifikke Integrerte Kretster (ASICs), en for hver krets. I tillegg er systemene verifisert ved hjelp av to ullike målinger. Først og fremst, en måling av forhørssonen, som er det området leseren er i stand til å lese en transponder. Deretter en måling av den utstrålte feltstyrken til hver system, både for å sjekke at systemene ikke overskrider grensene satt av ETSI, men òg for å få et dypere innblikk i hvordan hvert system yter.

Begge systemene oppnår en forholdsvis lang maksimumsleseavstand, 30 cm for halv dupleks (HDX) systemet og 15 cm for full dupleks (FDX-B) systemet, samtidig som de opprettholder en relativt begrenset fysisk størrelse. Dette gjør de ved hjelp av ferittantenner.

Table of Contents

Acronyms

ASIC Application Specific Integrated Circuit. iii, v, 27, 30, 31, 39, 40, 41

ASK Amplitude Shift Keying. 6, 42

CRC Cyclic Redundancy Check. 6, 7, 9

EAS Electronic Article Surveillance. 2

EIRP Equivalent Isotropic Radiated Power. 4

EMC Electromagnetic Compatibility. 21

EMI Electromagnetic Interference. 21, 40

ERP Equivalent Radiated Power. 4

EUT Equipment Under Test. 21, 25, 26, 34, 40

FSK Frequency Shift Keying. 8, 30, 42

GNSS Global Navigation Satellite Systems. iii, v, 1, 41

HF High Frequency. vii, 3, 4, 10, 11, 14, 17, 19

IFF Identification Friend or Foe. 2

IoT Internet of Things. iii, v, 42

ITS Intelligent Traffic Systems. 3, 4

LF Low Frequency. iii, v, vii, 1, 3, 4, 5, 8, 10, 11, 14, 21, 23, 27, 40, 41, 42

NFC Near-Field Communication. 3, 4, 10

NRZ Non-Return-to-Zero. 30, 32

NTNU Norwegian University of Science and Technology. i

OATS Open Area Test Sight. vii, 21, 22, 40

PCB Printed Circuit Board. 11, 31

RFID Radio Frequency Identification. i, iii, v, vii, 1, 2, 3, 4, 5, 8, 10, 11, 14, 16, 18, 19, 20, 24, 27, 40, 41, 42

UHF Ultra High Frequency. vii, 3, 4

Glossary

HDX Half Duplex Standard in ISO11784/5. iii, v, vii, viii, 5, 8, 9, 26, 30, 31, 35, 36, 38, 40, 41, 42

FDX-B Full Duplex Standard in ISO11784/5. iii, v, vii, viii, 5, 6, 7, 8, 9, 26, 27, 29, 31, 34, 36, 37, 39, 40, 41, 42

DBP Differential bi-phase-encoding. 6

UART Universial Asyncrhonous Receiver Transmitter, (Transmission/Receiver module for computer interfaces). 41

ETSI European Telecommunications Standards Institute,
organisation which mandates and standardises telecommunication within Europe. iii, v, 3, 21, 23, 24, 39

Microwave Radio systems which generally operates with
frequencies ranging from 0.3 GHz to 30 GHz. vii, 3, 4

Radar Radio detection and ranging, detection system which uses radio waves
for determining the distance, angle and radial velocity to objects. 2

SINTEF Norwegian Research institution. i, 23

2 Introduction

This project aims to explain the implementation of two long-range Low Frequency (LF) RFID readers, with physically small antennas. These readers are intended to be a proof-of-concept which indicates the possible configurations Nofence AS can use to read animal RFID transponders, to correlate them with their GNSS-based collars for livestock grazing. Additionally, the project aims to give a better insight into how LF RFID systems operate, and what is available as far as design parameters are concerned.

A concern with these GNSS collars is the connection between the specific collar and the animal's specific identification number. Seeing as livestock animals are in many countries mandated to be labeled using RFID ear tags, a solution to correlate collar ID with animal ID would be to scan these tags from the collar. An issue with this approach is the range of LF RFID, typically a transponder has to be within a few cm's from the reader's antenna for a successful scan. This read range can be increased using antennas with better magnetic properties, as well as increasing the transmit power and sensitivity of the receiver within the reader.

The current way of correlating device identity to animal identity, is manual and therefore has some points of failure. Additionally, it is inconvenient to the end-user, as just attaching the device to the animal can be a challenging task. The reading process of the tag is also not that simple as the numbers that are printed on the tag are printed in rounded text, and the entire identity number is a 12-digit number. If the animal is older the ink on the ear tag can be worn out and harder to read. The animals are also not likely to remain still while the end-user is reading and entering the numbers, which can lead to mistyping etc.

As stated a solution to these challenges is to scan the ear tag using an RFID reader circuit. These can either be done using a close proximity RFID reader, by scanning the tag as the collar is mounted on the animal, or it could be resolved using a long-range RFID reader which scans the tag remotely from the collar. The close proximity RFID reader is dependent on the end user performing the scan, which potentially opens for some human errors. While a long range RFID reader can potentially open for an automatic identity correlation, which does not need any interaction from the end-user.

Two long-range RFID readers are studied and implemented throughout this project, seeing as this can indicate whether an automatic implementation as described earlier is possible, Figure 1 illustrates how a long-range RFID reader could function.

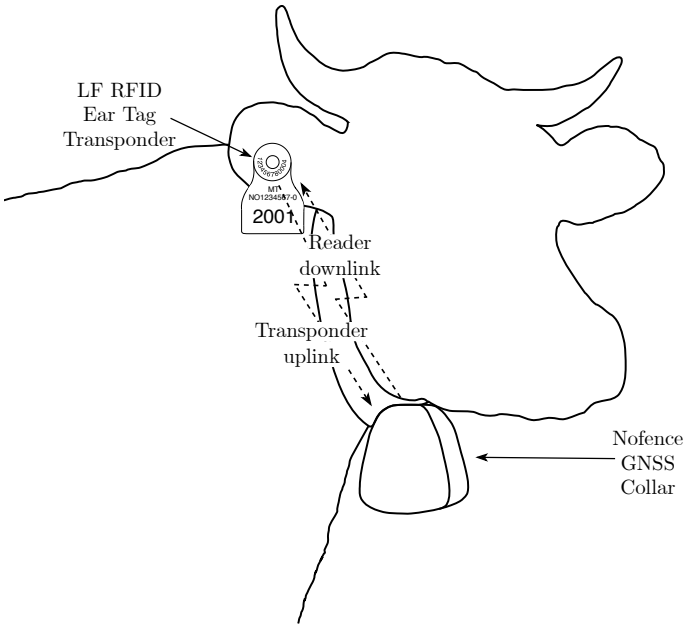

Figure 1: Illustration of a thought automatic solution

3 Theoretical Background

3.1 The history of Radio Frequency Identification (RFID)

RFID is in itself a combination of Radar and radio broadcasting technology.

Radar was developed after the first world war, to detect enemy airplanes from the ground. Soon after the deployment of airplane detection Radars, a concern with distinguishing between enemy and friendly planes emerged, which lead to the development of Identification Friend or Foe (IFF). IFF is a system that consists of a transponder located inside the airplane, which waits for an irrigation signal from the base station typically placed on the airbase. Once the transponder receives this signal, it transmits an uplink response to the base station confirming that it is a friendly airplane [1].

During the 1940s the first formalized research on the subject took place with Harry Stockmans 1948 Paper *Communication by the Means of Reflective Power*. This paper summarizes the then-current state of the principle, and that a lot of development was still required to make communication using reflected power feasible. The paper even mentions the possibility of using other media than radio waves: Soundwaves, Ultrasound, and light [2].

Stockman's paper lead to further research during the 50s and 60s, with the first commercial application of the technology, although not referred to as RFID, Electronic Article Surveillance (EAS), was released in 1966. The first development of EAS was considered to be relatively simple, using so-called 1-bit tags, which only allowed shopkeepers to know if an item with such a tag were present in the store or not. Later on, this application has become increasingly more advanced with individual labels on each item, which for example allows point of sale systems to update item count automatically of the particular item when it is sold [3].

In the 70s the RFID research became more focused on automation of different processes. Mainly factory automation, and toll collection as well as vehicle tracking. Many believe that it was due to the revolution of digital circuits which took place during the 70s that made the RFID development pick up the pace [3].

In the 80s the RFID became fully implemented, and the term RFID was first mentioned in the patent filed by Charles Walton in 1983. During the 80s the technology became commercially available to transportation systems, business applications, and animal tracking [4].

In the 90s RFID was already in such widespread use that standardization emerged. The technology became globally available despite it prior only being available for the U.S. and Europe [3].

During the 2000s more standards emerged, as well as the technology was improved which furthermore leads to the miniaturization of the technology [5].

3.2 RFID fundamentals

An RFID system in its most fundamental state consists of a reader, which operates similar to a base station in radio communications, and a tag also called transponder. RFID systems operate by the reader transmitting a radio wave or a magnetic field, which is often referred to as the downlink, to the tag. Inside the tag there is an antenna, and a radio transceiver front-end which ensures the uplink back to the reader. The tags antenna receives energy from the readers downlink which powers the transponder, when it has a sufficient magnetic field present, or is receiving enough energy from transmitted radio waves. Depending on the RFID standard used, and the architecture of the tag, the tag will operate either immediately when the readers downlink is present, (Full Duplex). Or the tag will have a energy harvesting circuit, which charges up a capacitor that then activates the uplink as soon as the downlink is finished, (Half-Duplex). The uplink to the base station is also referred to as tag response, and consists of a unique message for each individual tag. Whether the transponder is powered via a magnetic field or radio waves depends on the frequency used and the RFID standard used [5].

RFID technology operates using different frequency bands, the bands which are in current use, are abbreviated as LF, HF, UHF, and Microwave. Table 1 shows the abbreviations, and the frequency range at the bands, as well as some of the RFID applications currently in use at those specific bands.

Table 1: Frequency bands currently in use for RFID and NFC applications [5].

Band name	**Frequencies used** f	**Wavelength** λ	**Applications**
Low Frequency (LF)	124.2 kHz, 125 kHz & 134.2 kHz	2.2 km - 2.4 km	Access control, immobilizers Animal identification
High Frequency (HF)	13.56 MHz & 27.125 MHz	11 m - 22 m	**RFID:** Access control, tickets, Balises in railways **NFC:** Smart payment, device handshaking
Ultra High Frequency (UHF)	433 MHz, 860 MHz - 960 MHz	31 cm - 70 cm	Industrial automation Supply chain management
Microwave	2.400 GHz - 2.4835 GHz & 5.725 GHz - 5.875 GHz	5 cm - 12 cm	Electronic Tolling Collection, Intelligent Traffic Systems (ITS)

3.2.1 Low Frequency (LF)

All LF RFID systems use magnetic coupling as the physical layer for communication, this means that the transponder is powered via the magnetic field transmitted on the downlink from the reader. The RFID systems which operates on the LF band, operates on either 125 kHz or 134.2 kHz, where the latter is restricted to animal identification, either by implanted tags or exposed ear tags. RFID systems operating at LF have been standardized using the ISO/IEC 18000-2:2009 standard for devices operating with 125 kHz; and ISO11784/5 for 134.2 kHz devices. As the frequency range at which these systems are quite low, aspects like fading, where radio signals become deteriorated by surrounding objects and environment, become less of a concern, as the wavelength for these signals are quite large. Due to these aspects, the frequency band is considered to be quite ideal for animal identification RFID transponders. The signals will not become significantly deteriorated from things like mud,rain or dirt, and are not really affected by tissue and muscles so it can be implanted. In addition to this the standard is in use throughout the most of the world, for man owned animals, either livestock or household pets.

RFID systems operating in the LF frequency range are regulated as inductive coupled radio systems in Europe by the ETSI *EN 300 330 Standard*, which allows for a maximum radiated magnetic field strength of 66 dBµA/m, either measured or extrapolated at a distance of 10 m [6].

3.2.2 High Frequency (HF)

The most used band in RFID technology according to [5], is the HF band. This is due to the miniaturization capabilities of the system compared to the LF band, (loop antennas require fewer turns). Additionally, it is operating with magnetic fields as the physical layer, instead of radio waves, hence eliminating interference with other radio systems in wide use. Systems such as telecommunications or WiFi operate in the UHF and Microwave ranges using radio waves as the physical layer. The same does RFID systems operating in these ranges so cross-talk and interference are more of a concern here [5].

HF RFID main application is access cards. However, other applications such as train balises, used

for point communications for trains are another popular use of this band [5].

As mentioned HF RFID systems operate using a magnetic coupling similarly to LF, but at a higher frequency allowing for smaller antennas, (less turns on loop antennas), and operation at greater distances between reader and tag [5].

HF RFID is in Europe regulated by the *EN 300 330 Standard* and systems are restricted to maximum allowed field strength of 60 dBµA/m, at a distance of 10 m [6].

The HF band is also used by the newer NFC technology, which operates using the same principles as HF RFID, but the use cases are secure data transfers, in applications such as smart credit cards and handshaking between devices such as smartphones etc. [5].

3.2.3 Ultra High Frequency (UHF)

UHF RFID has in the latest 20 years received the most development, many producers advertise for readers being able to read tags at distances above 12 m. UHF RFID works more like a traditional radio-link, as the standard operates using radio waves instead of magnetic fields. This allows for more options in regards to antenna design, hence making it able to perform better in certain applications [5].

UHF RFID has multiple bands available for operations, which one is used is highly dependent on which part of the world the system is intended for. In Europe UHF RFID is regulated through the *EN 302 208 Standard*, and has the following available frequency bands: 865 MHz to 868 MHz with a maximum allowed radiated power 2 W Equivalent Radiated Power (ERP) and 915 MHz to 921 MHz with a maximum allowed radiated power 4 W ERP [7].

3.2.4 Microwave

Some RFID systems operate in what is often referred to as Microwave range. Most RFID systems that operate in the Microwave range are mostly operating on the frequency band 2.45 GHz which spans from 2446 MHz to 2454 MHz, as well as the 5.8 GHz frequency band spanning 5725 MHz to 5875 MHz. Typical RFID applications in the Microwave range are traffic tolling applications and Intelligent Traffic Systems (ITS). Most of the applications are based on the higher 5.8 GHz band as there are fewer other radio systems operating around that frequency band [5].

In this range, the frequency bands which are in use, also depend heavily on where in the world the system is intended for. However, Europe regulates Microwave RFID by the *EN 300 440 Standard* where the two bands listed above, 2.45 GHz and 5.8 GHz are regulated for RFID use. The 2.45 GHz band is allowed to have a radiated power of 500 mW Equivalent Isotropic Radiated Power (EIRP), and the 5.8 GHz band is allowed to have radiated power 25 mW [8].

3.3 LF RFID for Animal Identification

Most countries mandate labeling livestock animals with individual identity numbers to keep track of veterinary records, control and eradicate diseases as well as track the life cycle of a specific farming animal [9], [5]. Throughout the years this has been done in multiple ways, mainly burn marking, freeze marking, tattooing, and attaching ear tags, either electronic or non-electronic; and finally for some animals implanting an RFID microchip [5].

Visual tags and tattoo marks have existed for decades and are a cheap and practical method of labeling livestock animals. However, this method requires animals to stand still whenever the identity numbers are read out, which can be quite challenging as animal identity numbers can be up to 12 digits long. In addition to this, the labels can deteriorate over time which can deem them unreadable. Due to this RFID animal tags have been developed and are in extensive use. The RFID technology makes farmers able to reliably read out the identity numbers, as the RFID

tag will still hold the animal identity numbers within a memory unit regardless of how visible the printed tag is on the actual ear tag.

Another benefit of using ear tags instead of burn marking is animal welfare. As it is less painful for an animal to be labeled with an ear tag, than being labeled with burn marking. Additionally, ear tags require fewer resources per label than burn marking. Ear tags can also be reused as appose to an iron burn plate [10].

The most widespread RFID labels for livestock animal identification used are ear tags. This is due to their reusability, durability, and the fact that it is just an additional feature to print ear tags which already had existed before the development of RFID ear tags [10].

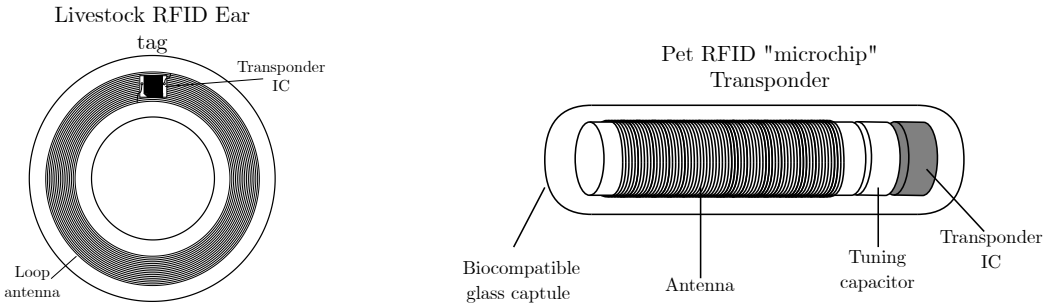

(a) Main components of an RFID Livestock ear tag transponder.

(b) Main components of an RFID "microchip" implantable transponder for household pets.

Figure 2: LF RFID transponder types for animal identification.

These tags consist of a loop antenna, which has two main functions: harvesting enough energy from the magnetic field transmitted from the reader, which powers the tag. As well as transmitting the response back to the reader. An illustration of how the internal components in such an ear tag transponder is shown in Figure 2a.

In addition to livestock, LF RFID transponders can be implanted in household pets and this is mandatory in many countries. Implanted transponders operate using the Full Duplex Standard in ISO11784/5. An illustration of such a transponder is presented in Figure 2b. Figure 3 shows a picture of an actual implanted tag, as well as the commercially available tags used within agriculture in Norway, and finally the internals of an ear tag.

(a) Internal of animal ID ear tag.

(b) OSID HDX ear tag.

(c) OSID FDX-B ear tag.

(d) Implanted RFID tag.

Figure 3: Different LF RFID tags for animal identification.

Other applications where LF RFID is used in immobilizer systems for vehicles, access control systems for buildings and even some car access systems [11].

3.3.1 Full Duplex Standard in ISO11784/5 (FDX-B)

The most common standard in use for LF RFID systems is the FDX-B standard. FDX-B is an abbreviation for full-duplex, implying that the reader and transponder operate at the same time.

This means that an FDX-B tag responds immediately whenever a reader's transmitted field is present and strong enough [12]. A shortcoming of this standard is that a transponders response can easily remain invisible to a reader if the readers uplink field is too weak compared to the reader's transmitted field.

3.3.2 Modulation and coding

The FDX-B standard is modulated using an Amplitude Shift Keying (ASK) modulation scheme. This means that the digital information bits are modulated with a varying amplitude to the carrier signal, similarly as to how an AM radio works. In addition to this FDX-B apply a coding scheme, Differential bi-phase-encoding or Manchester encoding as it is sometimes referred to. The digital signals are essentially coded in such a way that ("1")s have transitions for each symbol period, and ("0")s have transitions twice of that, each half symbol period [12]. The coding and modulation scheme for FDX-B is illustrated using Figure 4,

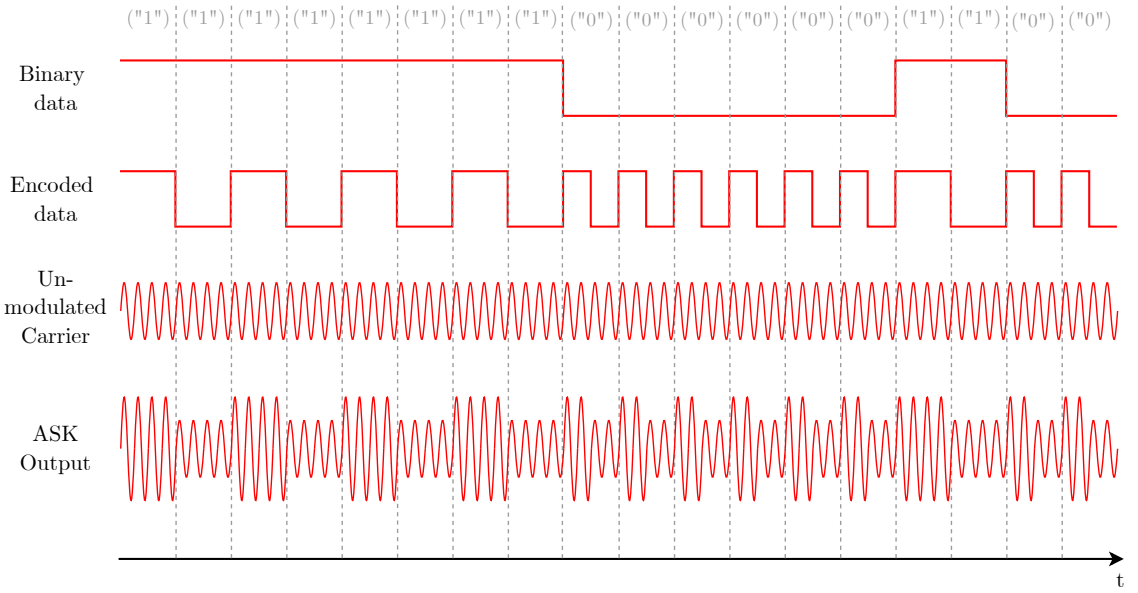

Figure 4: FDX-B coding- and modulation scheme.

3.3.3 FDX-B telegram layout

FDX-B transponders carry up to 128 bit of information and can be divided into the following blocks:

- 11 bit Header
- 64 Identification bits, with 8 additional control bits
- 16 bit CRC, with 2 additional control bits
- 24 bit of application specific data, with 3 additional control bits

The 11 header bits are used to indicate an incoming data transmission from tag to the receiver, and is differentiated from the remaining data by the use of the control bits before each following byte. The 64 bit identification block consists of 38 bit representing the 12-digit identification printed on tags, 10 bits represent the 3-digit country code in accordance with *ISO3166* [13], 2 bytes currently only in use for setting data block status flag and the application indicator flag. The data block status flag is set if the 24 bit data block after the CRC contains any information, ("1") if there is information, ("0") if not. The application indicator flag is used to indicate whether a transponder

is used for animal identification or not: ("1") if used for animal identification, ("0") if not. The reader has to perform a CRC over the 64 bit identification block, before correlating this with the 16 bit CRC block. After the CRC block, the additional data block proceeds, if in use it can store parameters like weight, age, etc. for the individual livestock animal. These features are used in automatic feeding systems, so animal welfare parameters are met [12] [14].

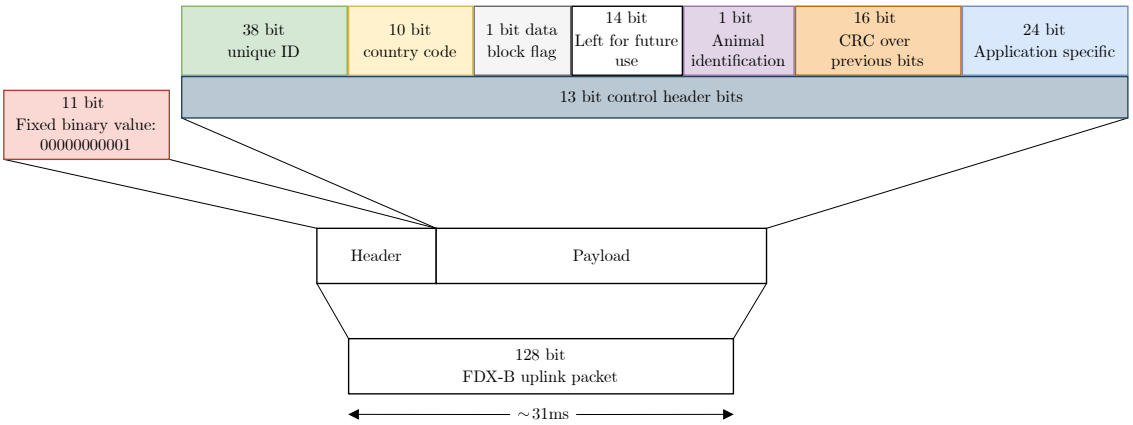

Figure 5: FDX-B telegram layout.

Figure 5 illustrates how the up-link telegram format. Figure 6 shows an example of the binary data layout in these telegrams. What is special is that the order of bytes are is flipped they are sent out, so to be able to correctly read out the information from the transponder, one has to read byte vise from right to left.

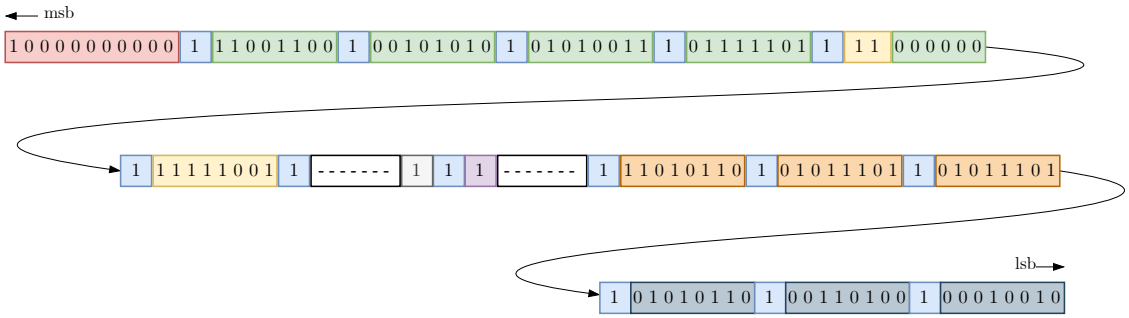

Figure 6: FDX-B telegram layout, example.

A correct readout from Figure 6 yields the resulting structure presented in Figure 7 when read from byte 4 to 1:

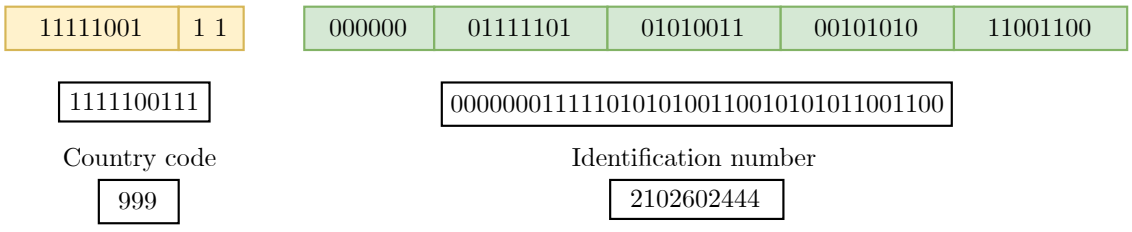

Figure 7: FDX-B readout example.

3.3.4 Half Duplex Standard in ISO11784/5 (HDX)

The other common protocol used for LF RFID livestock ear tags is the HDX protocol. This protocol is also defined in the ISO11784/5 standard, and operates differently from the FDX-B protocol. As described in Section 3.3.1 FDX-B transponders transmit immediately when a magnetic field with enough strength is present, a HDX transponder works differently as it uses the magnetic field to charge an internal capacitor present in the transponder. When the magnetic field from the reader is switched off the HDX transponder will transmit the uplink signal to the reader. As this uplink signal will not be placed on top of a strong reader transmitted field, the uplink will be simpler to detected at a greater distance than for a FDX-B transponders uplink [15].

3.3.5 Modulation and coding

The HDX protocol is defined to operate at the 134.2 kHz band. The protocol also employs a Frequency Shift Keying (FSK) modulation scheme, where ("1")s are transmitted at 124.2 kHz and ("0")s are transmitted at 134.2 kHz. More specifically the standard regulates the binary values to be modulated as 16 cycles at each frequency, i.e. ("1")s correspond to 16 cycles at 124.2 kHz, and ("0")s correspond to 16 cycles at 134.2 kHz.

In contrast to the FDX-B protocol, the HDX protocol does not employ any coding scheme to the signal.

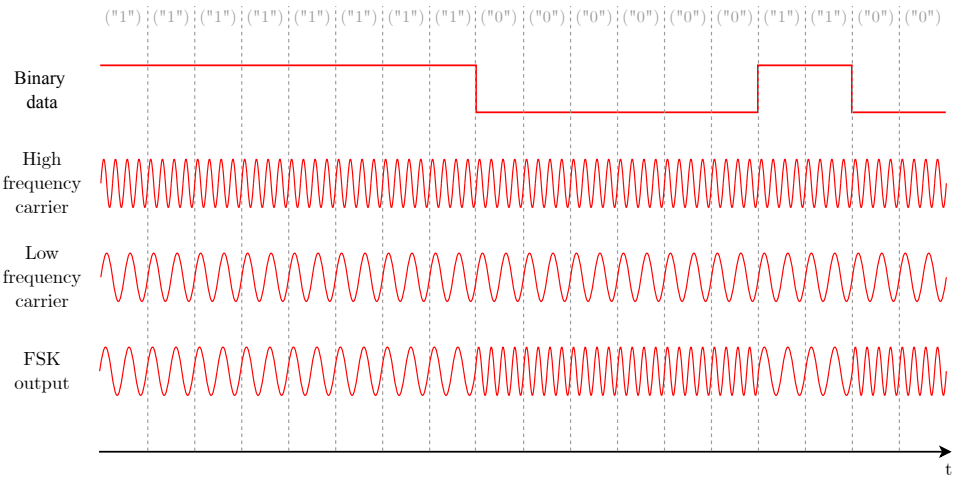

Figure 8: example of HDX uplink signal generation using FSK.

For communication from reader to transponder to take place, the transponder as mentioned needs a charge up field from the reader to operate. After the transponder has been sufficiently charged it is able to uplink to the reader. The communication principle is visualized in Figure 9

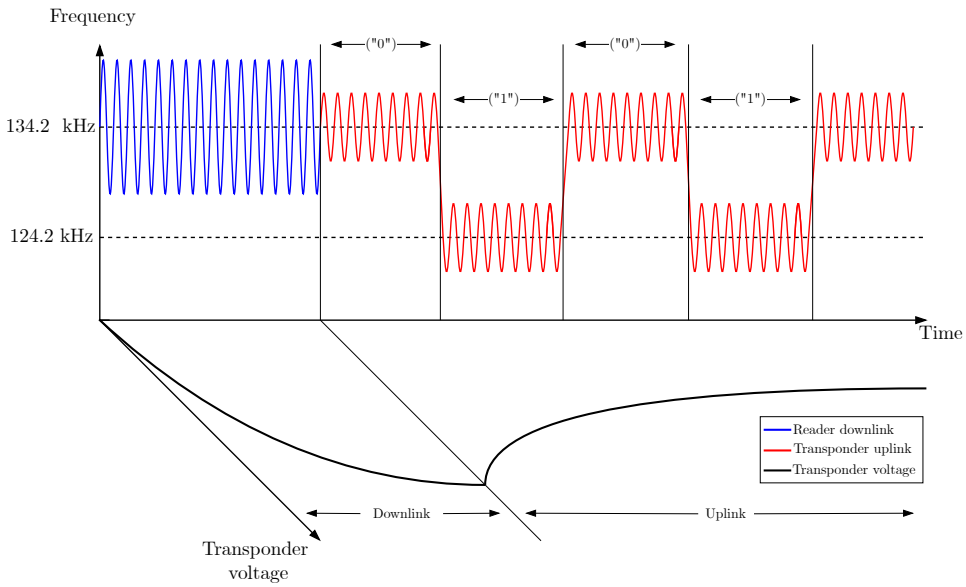

Figure 9: HDX communication principle, based on [16].

3.3.6 HDX telegram layout

Similarly to the FDX-B protocol described in Section 3.3.3, the HDX protocol consists of a 38 bit identification block, 10 bit nation code, 1 bit data block flag, 1 bit application flag, 16 bit CRC and finally 24 bit data block for optional information storage. In contrast to the FDX-B protocol the HDX protocol does not have control bits in the beginning of each byte. The header is also different, as it is only 8 bit long, and has different fixed value in comparison to the header found in the FDX-B standard. Due to the shorter header and lack of control bits, the HDX uplink packet has a size of 112 bit. Figure 10 illustrates the layout of the uplink telegram from transponder to reader. The layout similar to the FDX-B protocol, but lacks the control bits, and has a smaller header [15].

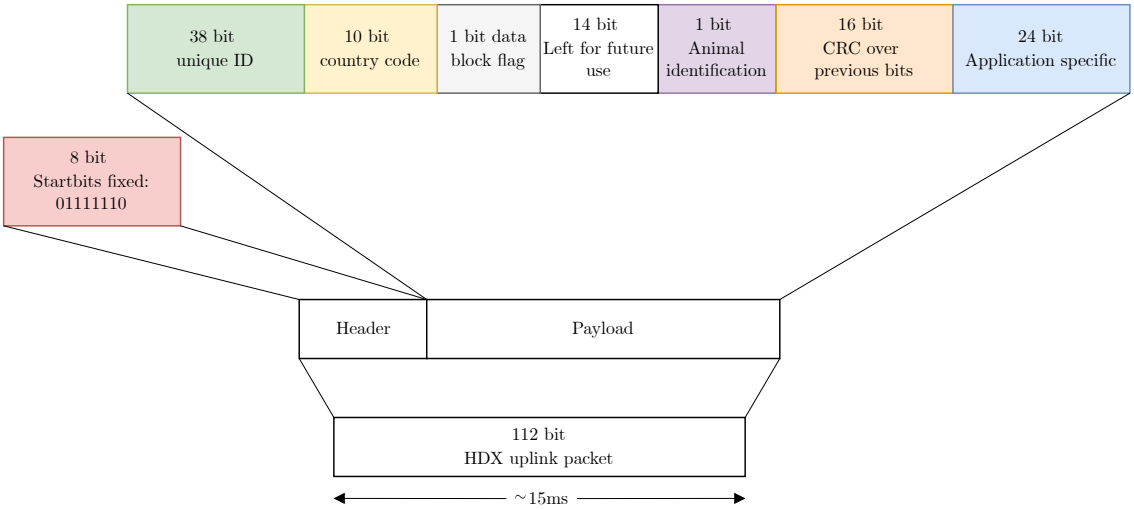

Figure 10: HDX telegram layout.

3.4 LF RFID Antennas

An integral part of any RFID system is the antenna. Antennas are frequency-dependent components, and as Table 1 shows, the wavelength λ for the LF band ranges from 2.2 km to 2.4 km. If a classic half-wave dipole antenna were to be crafted for this frequency range it would be just over a kilometer in length. Regardless of this antennas used in HF and LF RFID, as well as NFC devices, can be crafted to be less than the size of a grain of rice. Fitting an antenna in such a limited dimension will simply lead to all antennas being considered electrically extremely small. A consequence of this is that the radiation efficiency will be around 0. This means that looking at typical antenna parameters such as radiation resistance and antenna gain does not really make sense. The way that these systems operate, as appose to a normal radio system, is by inductive coupling. This means that the most important property of these antennas is their ability to generate a magnetic field. Antennas for these systems are therefore optimized for their magnetic properties [17] [5].

The physical orientation of antennas is often referred to as axial and radial directions. The axial direction means the direction of the axis of the antenna, and the radial direction means the direction in the radius of the antenna. This is illustrated for the two main antennas used in this thesis with Figure 11.

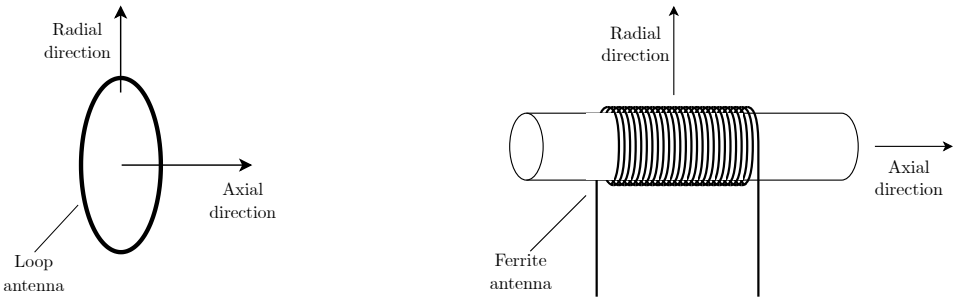

(a) Physical orientation of loop antenna.

(b) Physical orientation of ferrite antenna.

Figure 11: Physical orientations of antennas used with LF RFID.

3.4.1 Air loop, Magnetic loop

Air loop antennas are normally used for readers in LF and HF RFID systems. Loop antennas are often used as they are cheap to manufacture, can be made with high levels of accuracy and are adaptable to mechanical designs. As stated, the most important aspect of an LF RFID systems antenna are the magnetic properties, and the inductance of the antenna is the most important property. This is caused by the fact that the magnetic **B** field i.e. the magnetic flux density is proportional to the inductance L in the antenna [5].

3.4.2 Inductance of an n turn loop

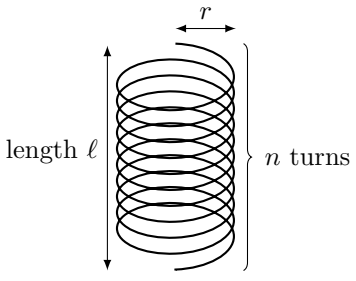

Figure 12: n turns air core loop, with length ℓ and radius r.

The inductance of an air loop antenna as illustrated in Figure 12 can be estimated with Wheelers formula [18]

$$L \approx \frac{10\pi\mu_o n^2 r^2}{9r + 10\ell}, \tag{1}$$

where
L is the inductance given in µH
n is the number of turns
r is the radius of the coil
ℓ is the length of the coil
μ_0 is the permeability of vacuum, $\mu_0 = 4\pi{\cdot}10^{-7}$ H/m.

This is a relatively inaccurate approximation and it is only valid for coils which have an aspect ratio of at least 0.8, meaning that the length ℓ has to be at least 80% of the coil's radius r [18].

For a loop antenna intended for use within an LF or HF RFID system, the length is seldom 80% of the radius since these systems often require antennas to be etched onto a PCB or placed around the perimeter of a thin device. Due to aspects like this, more accurate formulas have since been developed. In the same source, [18], a more accurate formula is listed, it claims to be within ± 265ppm for any given geometry

$$L = \mu_o r n^2 \left[ln\left(1 + \frac{\pi}{2(\ell/d)}\right) + \frac{1}{2.3004 + 3.2219(\ell/d) + 1.7793(\ell/d)^2}\right], \tag{2}$$

where
d is the diameter of the coil ($d = 2r$)
(ℓ/d) is the aspect ratio of the coil.

3.4.3 Near field of an electrically small loop antenna

Given that a loop antenna is placed horizontally in the xy-plane, with its axis is pointing in the z-direction, the near field components of electrically small loop antennas can be described in spherical coordinates as [19]

$$E_r = E_\theta = H_\phi = 0 \tag{3}$$

$$E_\phi = \eta \frac{(ka)^2 I_0 sin\theta}{4r}\left[1 + \frac{1}{jkr}\right] e^{-jkr} \tag{4}$$

$$H_r = j\frac{(ka)^2 I_0 cos\theta}{2r^2}\left[1 + \frac{1}{jkr}\right] e^{-jkr} \tag{5}$$

$$H_\theta = -\frac{(ka)^2 I_0 sin\theta}{4r}\left[1 + \frac{1}{jkr} - \frac{1}{(kr)^2}\right] e^{-jkr}, \tag{6}$$

where
I_0 is the constant current distribution along the loop
k the wave number ($k = \frac{2\pi}{\lambda}$)
a the radius of a loop placed in the xy-plane
η the intrinsic impedance ($377\,\Omega \simeq 120\pi\Omega$ for free-space)
E_r radial distance of the electric field

E_θ polar angle of the electric field
E_ϕ azimuth angle of the electric field
H_r radial distance of the magnetic field
H_θ polar angle of the magnetic field
H_ϕ azimuth angle of the magnetic field.

Equation 5 and Equation 6 govern the distribution of magnetic field in the Near-Field. As there are two magnetic field components as appose to one electric field component, Equation 4, the magnetic loop has a dominating magnetic field in the Near-Field region, which another desired property for inductive coupled system. Figure 13 shows the magnetic field of a loop antenna placed in the xy-plane, with the axial direction pointing upwards in the z-direction,

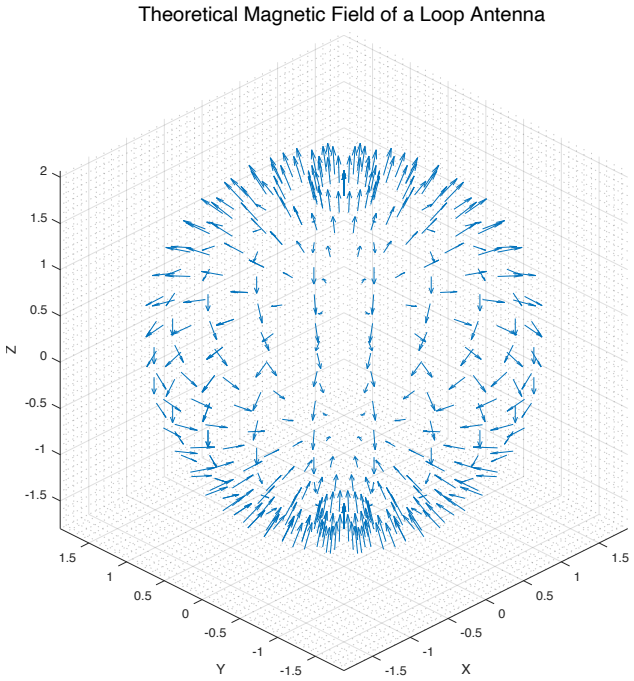

Figure 13: Magnetic field of a loop antenna placed in the xy-plane, with the axis pointing in the z-direction.

3.4.4 Ferrite loop antenna

Ferrite loop antennas operate similarly to an air loop antenna, but the key difference is the introduction of the ferrite core, which the loop is wrapped around. The main purpose of the ferrite core is to simply increase the magnetic permeability of the antenna. The ferrite core will do this as long as the ferrite material has a higher permeability value than the free space permeability μ_0.

Due to the increase in permeability, the antenna can be made smaller in physical size in comparison to an air-core equivalent. However as the magnetic flux will not be fully contained within the ferrite material, as some parts of the flux will be in the air around the core, the calculations become more complex and less accurate. The mechanical dimensions used for estimating the inductance of a ferrite core loop are summarized in Figure 14

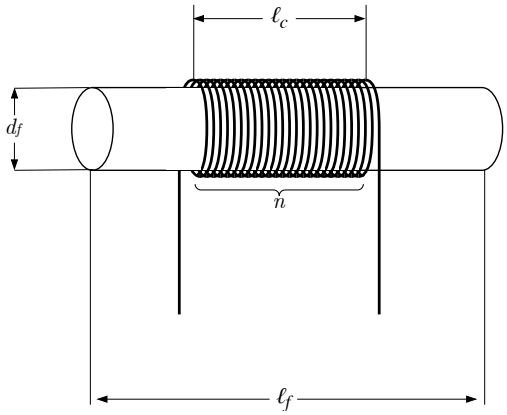

Figure 14: Mechanical dimensions for ferrite antennas.

3.4.5 Ferrite Material

The ferritic material determines how permeable the antenna will be at different frequencies. Ferrites are classified as a ceramic material, containing a combination of iron(III)oxide (Fe_2O_3) and another metallic element. These other metallic elements can be magnesium, nickel or zinc to name a few. Ferrites are manufactured by mixing and firing large amounts of (Fe_2O_3) with the additional metal, the ratio of (Fe_2O_3) and the additional metal is manufactured to suit different applications. This also is dependant on the additional metal. Due to different amounts of (Fe_2O_3) ferrites are often classified into the following 3 classes: **Soft ferrites**, **Semi-hard ferrites** and **Hard ferrites** [20].

For radio applications soft ferrites has the most suited properties. These properties are namely: High resistivity, low losses and low hysteresis loss. The high resistivity prevents eddy currents in the material, which essentially limits losses. The low hysteresis loss is caused by the low coercivity the material has, coercivity is essentially defined as the ability a material has to withstand an external magnetic field without becoming demagnetized [21].

A common soft ferrite type is manufactured from manganese (Mn) and zinc (Zn). These ferrites has the chemical formula: ($Mn_aZn_{(1-a)}Fe_2O_4$) and are suited for radio applications operating at a frequency ranging from 0 Hz up to 1 MHz. Another common soft ferrite type is the Nickel-Zinc (NiZn) type, which has the chemical formula: ($Ni_aZn_{(1-a)}Fe_2O_4$). (NiZn) ferrites are suited for radio applications operating at a frequency above 1 MHz [20].

An important property explaining the effect that high frequencies has on the magnetic properties of a material is the complex permeability. This is a metric of the ratio between the B field and H field, which in terms is the ratio between the magnetic flux density and the magnetic field strength. If the fields are described as phasors it can be shown that the loss tangent, which is the ratio of how much power is lost in the material vs. how much is stored can be written as [22]

$$tan(\delta) = \frac{\mu^{''}}{\mu^{'}} \tag{7}$$

where
δ is the phase delay from B to H
$\mu^{'}$ is the real part of the permeability
$\mu^{''}$ is the complex part of the permeability.

3.4.6 Inductance of Ferrite Loops

An article published by [23] proposes a new way of estimating the inductance of loop antennas wound around ferrite rods, as most established methods often yield inaccurate results. This article compares the common approaches with simulations and measurements and proposes a new

approach based on its results. A term that is normally used when calculating the inductance of a ferrite antenna is the permeability value (μ_{coil}) which is the ratio of the inductance with and without a ferrite core on a loop antenna. This is a term that is of limited value as the inductance of an air-core antenna is very dependent on factors such as coil and wire diameter. Another issue with established methods is that there are often quite many terms that have to be calculated before the actual inductance can be calculated [23].

The article published by [23] proposes the following equation

$$L = A_L n^2, \tag{8}$$

where
L is the inductance of the antenna, [H]
A_L is the so called inductance factor, $[\mathrm{H}/n^2]$
n is the number of turns.

The A_L term includes the permeability of the ferrite material (μ_i), length of the ferrite (ℓ_f), and its cross-sectional area (A_f). According to [23], this factor is found in many places in literature and is often calculated as

$$A_L = \mu_o \mu_{rod} \frac{A_f}{\ell_f} \tag{9}$$

where
μ_0 is the permeability of vacuum, $\mu_0 = 4\pi{\cdot}10^{-7}\,\mathrm{H/m}$
μ_{rod} is the fluxmetric permeability, which is only applicable to full length coils, i.e. ($\ell_c = \ell_f$)
(ℓ_c) is the coil length.

Due to this [23] proposes a new method for determining the (A_L) term using a replacement of the (μ_{rod}) term with a term (μ_L) called *inductive permeability*. The new proposed equation is denoted as

$$A_L = \mu_o \mu_L \sqrt{\ell_f d_f}, \tag{10}$$

where
μ_L is the relative permeability of the antenna
ℓ_f is the length of the ferrite rod, as shown in Figure 14
d_f is the diameter of the ferrite rod, as shown in Figure 14.

The relative permeability term (μ_L) is a function of coil length (ℓ_c), rod aspect ratio (ℓ_c/d_f), and the intrinsic permeability of the ferrite material (μ_i). The ratio of coil length to rod length ($\ell_c \ell_f$) accounts for most of the variation in μ_L. The intrinsic permeability and rod aspect ratio play less of a role, but are still significant.

A MATLAB script is bundled with the article from [23] for estimating (μ_L) together with (A_L). Using the ferrite rods diameter (d_f), length (ℓ_f), intrinsic permeability (μ_i), and the length of the coil wound around the ferrite rod (ℓ_c), as input arguments, the relative permeability μ_L is extrapolated from a data set that is based upon multiple electromagnetic simulations.

3.5 Electrical Resonance

Electrical resonance or a tuned circuit is a fundamental building block in many electrical or electronic systems in use today. This is also a fundamental building block in both transponder and reader for HF and LF RFID systems. A resonant circuit typically constructed with a resistive element R, a capacitive element C, and an inductive element L.[24] The combined frequency response

characteristic of the elements will in a tuned circuit have a similar behavior to the one shown in Figure 15,

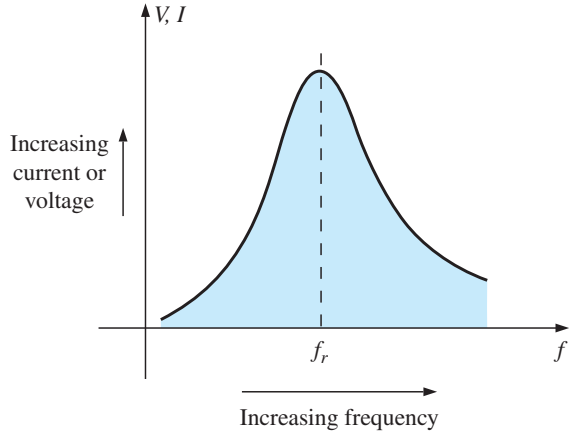

Figure 15: Tuned circuit typical frequency response characteristic [24].

3.5.1 Series- & Parallel Resonance

There are two types of resonant circuits, these are *series* and *parallel*. The circuits can essentially be modeled as shown in Figure 16, where Figure 16a shows series resonance response and the Figure 16b shows the parallel response.

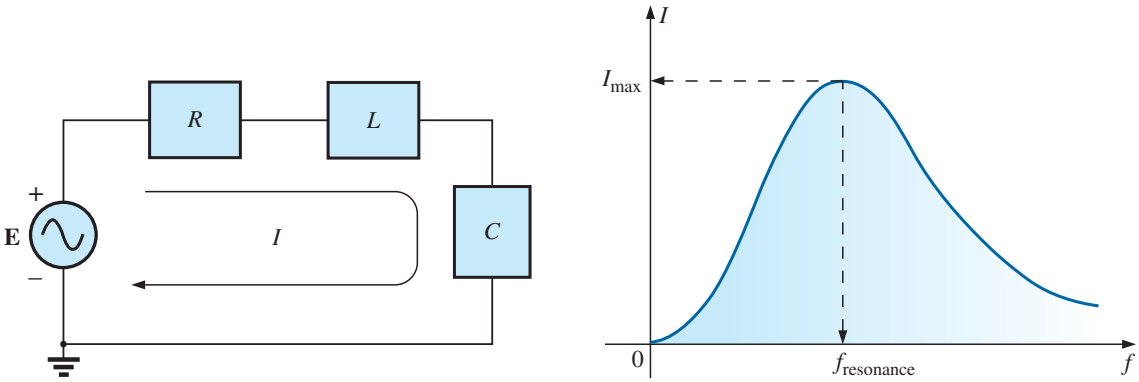

(a) Series network.

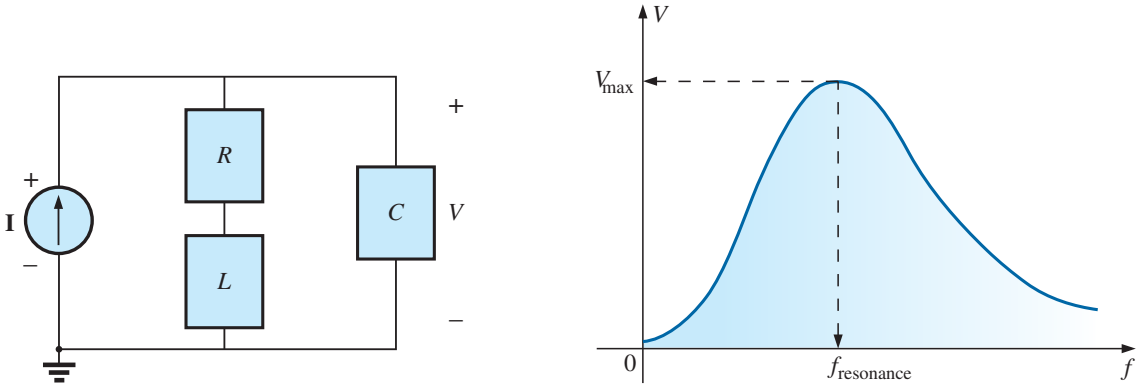

(b) Parallel network.

Figure 16: Series and parallel networks with their resonant curve of interest [24].

Both of these networks feature a resonant characteristic, however, the series network features a

current maximum at resonance, and the parallel network has a voltage maximum at resonance [24].

Resonance occurs whenever the reactive part of the inductive element equals the reactive part of the capacitive element, leading to a purely resistive circuit. As both inductors and capacitors are frequency-dependent components, this phenomenon will occur at a certain frequency where the inductive element equals the capacitive. Thomsons equation describes the frequency where this phenomenon occurs [24] [5]

$$f_{res} = \frac{1}{2\pi\sqrt{L \cdot C}}, \tag{11}$$

where
f_{res} is the resonance frequency [Hz]
L is the inductance of the circuit [H]
C is the capacitance of the circuit [F].

3.5.2 Resonance in RFID transponders

According to [5] an RFID transponder can be modeled as the circuit presented in Figure 17, where the transformer coupled between L_1 and L_2 is represents the antennas for the transponder and reader, R_2 is the non-ideal resitive part of the transponders antenna, C_p is the parallel tuning capacitor for the transponders analog front end. The gray box containing the R_L and C_2' is modelling the microchip within the transponder, where R_L models the current draw, and the C_2' is the parasitic capacitance associated with the microchip. The AC voltage source $\underline{u}_{Q2}$ models the induced voltage within the resonance circuit.

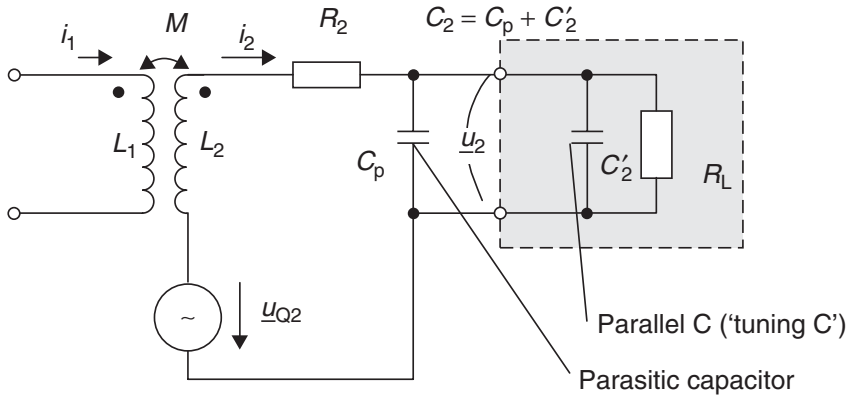

Figure 17: Equivalent circuit for magnetically coupled conductor loops [5].

It can be shown that the induced voltage in the circuit from Figure 17 can be mathematically described as

$$u2 = \frac{\omega \cdot k \cdot \sqrt{L_1 L_2} \cdot i_1}{\sqrt{\left(\frac{\omega L_2}{R_L} + \omega R_2 C_2\right)^2 + \left(1 - \omega^2 L_2 C_2 + \frac{R_2}{R_L}\right)^2}}, \tag{12}$$

where
ω is the angular frequency ($\omega = 2\pi f$)
i_1 is the current in the transmitter antenna [A]
k is the coupling coefficient for between L_1 and L_2.

If the transmitter current i_1 together with the inductances L_1, L_2 and resistances R_2, R_L are held constant, a frequency sweep can be applied to Equation 12. Figure 18 shows a plot from a simulation where this has been done, the solid curve displays the induced voltage behaviour with the tuned resonance circuit. In this characteristic. The dashed curve displays the induced voltage on the coil without the resonance circuit.

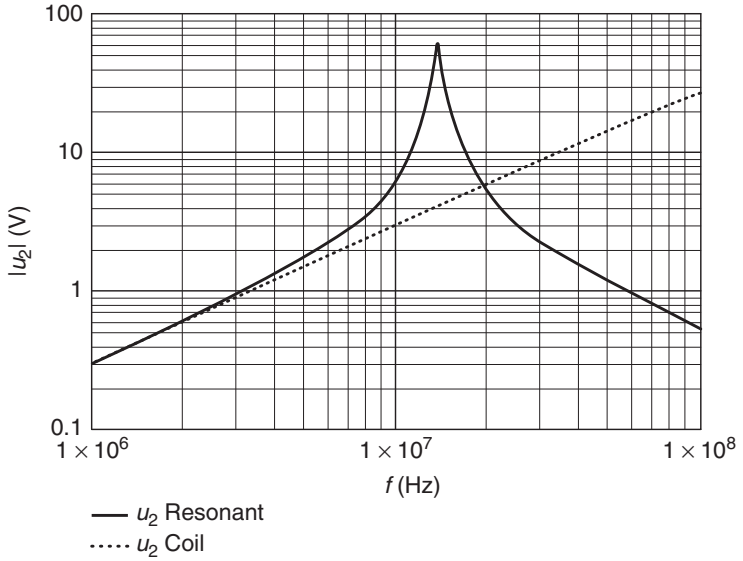

Figure 18: Voltage induced in a transponder coil with and without the resonance circuit vs. frequency, model is a HF transponder with the resonant frequency ($f_{res} = 13.56\,\text{MHz}$) [5].

3.5.3 Q factor

Another important concept with resonance electrical circuits is the Q factor. The Q factor is a measure of the step-up in either voltage or current in a resonant circuit at its resonant frequency. It is defined by the ratio of the reactive power in the reactive element to the average power of the resistive element [24]. For a series RLC-network the quality factor is defined as, [25]

$$Q = \frac{1}{R}\sqrt{\frac{L}{C}} = \frac{\omega_0 L}{R} = \frac{1}{\omega_0 RC}, \tag{13}$$

where
R is the resistive element of the resonance circuit
C is the capacitive element of the resonance circuit
L is the inductive element of the resonance circuit
ω_0 is the angular resonance frequency of the circuit.

For a parallel network, the Q factor becomes the inverse of the series case

$$Q = R\sqrt{\frac{C}{L}} = \frac{R}{\omega_0 L} = \omega_0 RC. \tag{14}$$

The Q factor is closely related to the bandwidth of a system if the Q factor is very high it will result in a very narrow bandwidth of the system. If the Q factor is lowered the system will have a wider bandwidth, but with a lower voltage/current step up. Figure 19 shows the effect of tuning the Q factor of a resonant series RLC network where the L and C element is held constant while the R element is changed [24].

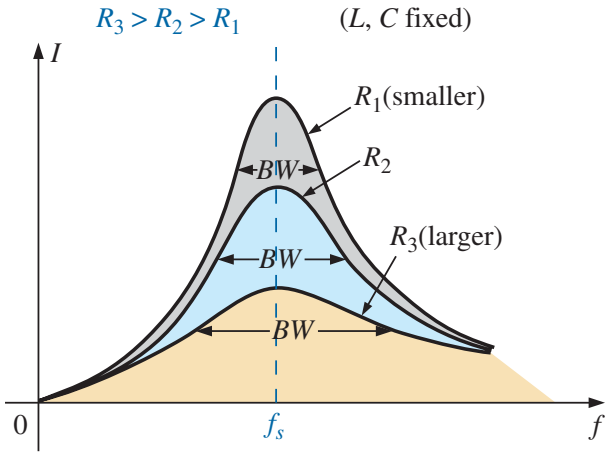

Figure 19: Effect of different resistive values on the bandwidth and step up of a series RLC network [24].

3.6 Magnetic Fields and the Interrogation Zone of RFID Readers

In inductively coupled RFID systems, magnetic antennas are used to generate alternating magnetic fields which the systems use as a physical layer for communication. If a measuring point is established in the center of the axial direction of such a magnetic loop antenna, (z-axis in Figure 13), the magnetic field strength will have similar behavior to the one in Figure 20. Where the magnetic field strength will have a low-pass characteristic, meaning that the magnetic field strength will remain almost constant until a certain distance where it then will be dampened by approximately 60 dB per decade [5].

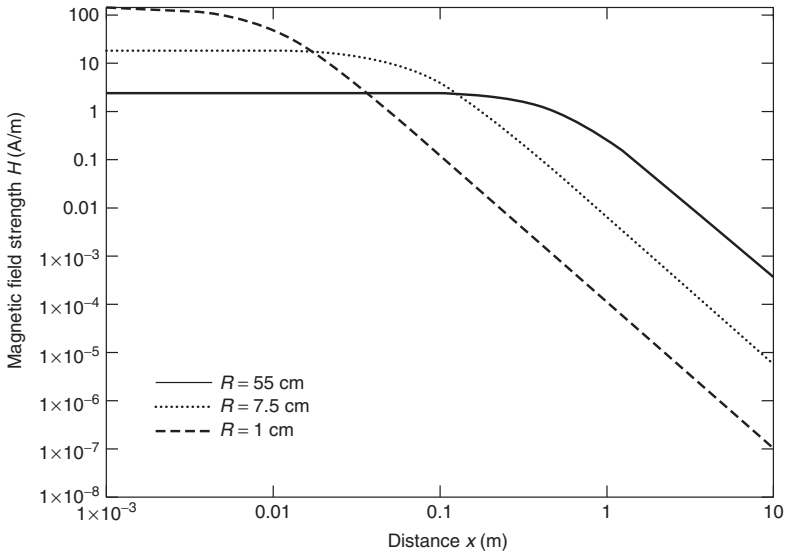

Figure 20: The dampening of the magnetic field strength, created by three different magnetic antennas, where the current and number of turns are held constant for each antenna, as the range from the antenna is increased logarithmically [5].

This effect is observed in the near field of such a magnetic loop where the field strength in the axial direction essentially follows a factor of $1/r^3$, this correlates with the near field equations from Section 3.4.3. In this region an electric field will also increasingly develop by induction, which results in the field turning from almost magnetic into electromagnetic as the distance from the antenna is increased. At a certain distance, the electromagnetic field will exist independently of

the antenna and hence have turned into an electromagnetic wave. this is known as the far-field. An important property in this region is that the electromagnetic wave can not retroact upon the antenna which created it. For an inductively coupled RFID system, this is important since an inductive coupling cannot exist when this effect has taken place. After the transition from near-field to far-field has occurred and the magnetic field is dampened by a $1/r$ factor which results in a dampening of 20 dB per decade. This is caused by the fact that the $1/r^3$ factors from Equation 5 & Equation 6 in the far-field, is too small to affect the field. Figure 21 illustrates the dampening of the magnetic field in the near field and far-field regions [5].

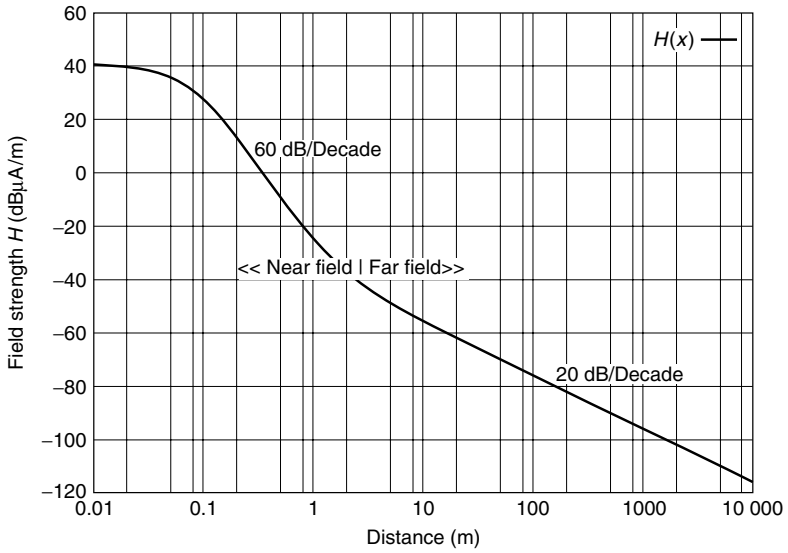

Figure 21: Magnetic field strength of a loop antenna measured in the axial direction of the antenna, from the near to far field region, with a resonance frequency of 13.56 MHz (HF) [5].

Another important aspect of inductively coupled systems is the so-called interrogation zone. This is known as the area around a reader where the transponder can be magnetically coupled. This area is highly affected by the orientation of both reader and transponder relative to each other, as the magnetic fields generated by each device will affect the other. If the transponders axial direction is slightly tilted away from the axial direction of the reader, the relationship in very general terms will follow

$$u_{0\vartheta} = u_0 \cdot cos(\vartheta), \tag{15}$$

where
u_0 is the induced voltage when the transponder axis is normal to axis of the reader
ϑ is the displacement angle between the readers axis and the transponders axis
$u_{0\vartheta}$ is the induced voltage when the transponder is tilted in relation to the readers axis.

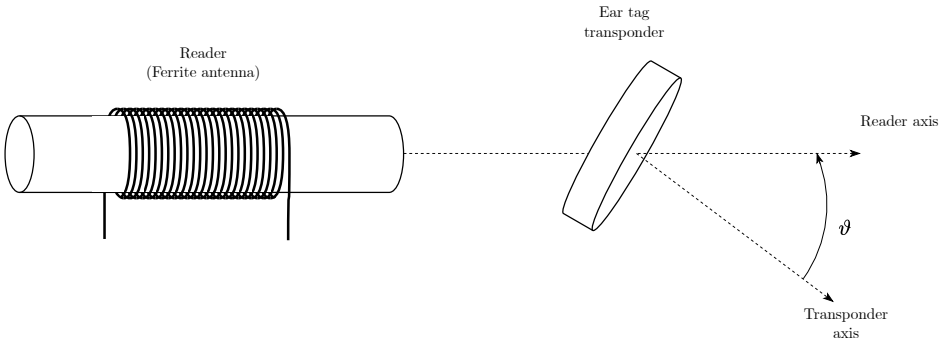

Figure 22: Illustration of the displacement between the axis of the readers antenna and the transponders antenna, based on [5].

At an angle $\vartheta = 90°$ where the magnetic field lines will run in the plane of the coil, no voltage will be induced.

As a result of the bending magnetic field lines in the entire area around the reader coil, in addition to the angle ϑ of the magnetic field H, will lead to the characteristic interrogation zone which is illustrated in Figure 23 [5].

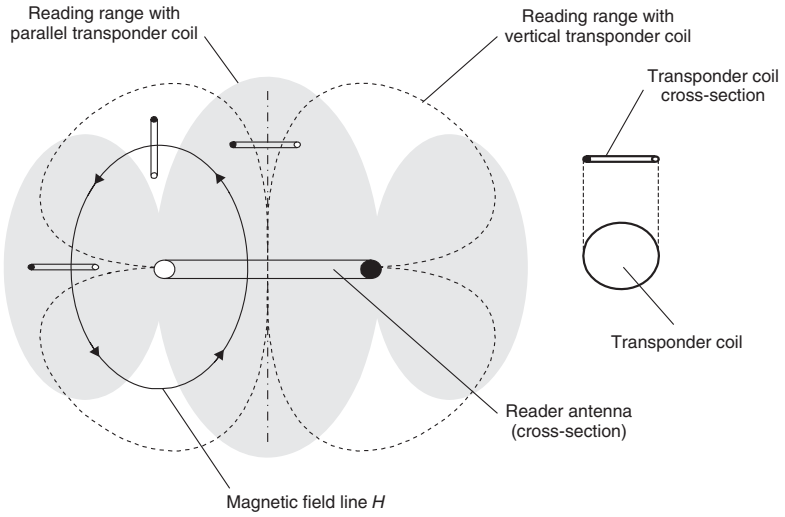

Figure 23: The interrogation zone of an RFID reader with different alignments of a transponder [5].

The interrogation zone is greatly affected by the orientation of the transponder, if the axial direction of the transponders antenna is placed normal to the axial direction of the reader antenna, the gray interrogation zone of Figure 23 will be present. If the axial direction of the transponders antenna is placed perpendicular to the axial direction reader, a completely different interrogation zone emerges. Then the area enclosed by the dashed line from Figure 23 will be present [5].

3.7 Antenna Factor (AF) & Free Space Impedance (Z_0)

The antenna factor is a fundamental metric of a calibrated antenna. The metric is defined as the relationship between the electric field present E and the induced antenna voltage V_{ant} [26]

$$AF = \frac{E}{V_{ant}}. \tag{16}$$

This is an important metric for Electromagnetic Interference (EMI) and Electromagnetic Compatibility (EMC) testing, as this relationship can be implicitly used to measure the radiated field strengths of a device. However the field present at the antenna terminals is not the explicit electrical field, due to loading effects, aperture characteristics of the antenna and the antenna gain [26].

Another important relationship in this domain is the free space impedance Z_0 which is fundamentally the relationship between the electric field E and the magnetic field H

$$Z_0 = \frac{E}{H}, \tag{17}$$

where
Z_0 is the free space impedance, $Z_0 \approx 377\,\Omega$
E is the electric field [V/m]
H is the magnetic field [A/m]

This relationship is useful for measuring a magnetic field using a magnetic antenna, as it implicitly measures the magnetic field strength [26].

3.8 Field measurements

As stated in Section 3.2.1, the *EN 300 330 Standard* limits the maximum allowed magnetic field strength transmitted to be 66 dBµA/m measured at a distance of 10 m for inductive systems. Where a measurement distance of 10 m is not possible, a measurement at 3 m can be done, where the resulting measurement is extrapolated to 10 m distance. To validate that a system does in fact not violate this specification, the *EN 300 330 Standard* lists means of measuring the field strength. For a transmitters it is firstly important to classify it correctly [6].

The standard classifies transmitters to be inductive if the following characteristics are met:

- The loop antennas area A is $< 30\,\mathrm{m}^2$
- The length of the loop l shall either be $< \frac{\lambda}{4}[m]$, $< \frac{75m}{f}[m]$, where f is given in MHz, or finally < 30 m. Which ever of these three requirements which is shortest in length.
- The antenna coil is allowed to have either one or multiple turns.

The standard further suggests the following equipment for measuring transmitted H-fields:

- A shielded loop antenna with known characteristics.
- A measurement receiver, this can be a spectrum analyzer, an oscilloscope, a powermeter or any other equipment suitable for measuring the transmitted field from the Equipment Under Test.

ETSI also requires the measurements to be done in an appropriate environment. The standard lists three different test environments, an anechoic chamber, an anechoic chamber with a conducting ground plane, and an Open Area Test Sight (OATS). The OATS is the environment that is suitable for LF inductively coupled systems [6]. ETSI differentiates *relative* measurements from *absolute* measurements. Where *absolute* measurements have to be carried out at verified test sights, with professionally calibrated measurement setups.

3.9 Open Area Test Sight (OATS)

OATS are generally suited for measurements in the frequency range from 9 kHz to 1000 MHz. A test sight like this should ideally have a rotateable antenna turret at one end and a fixed antenna mast with variable height at the other [6].

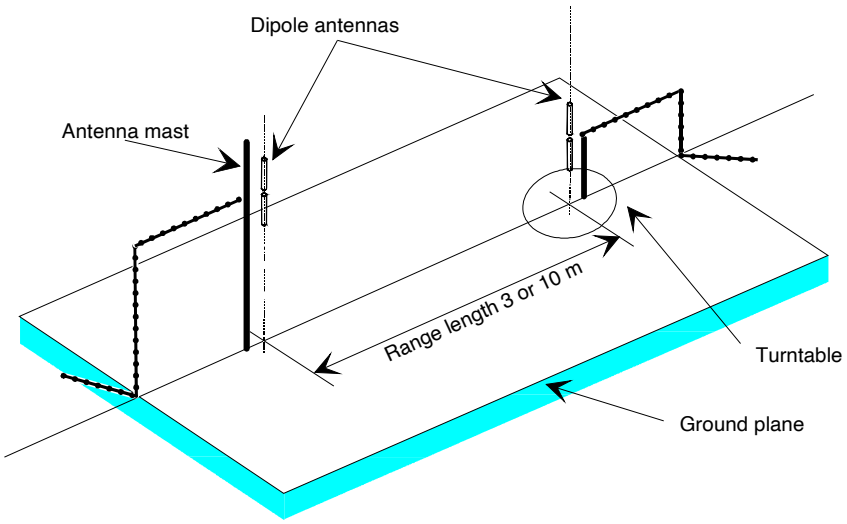

Figure 24: Illustration of an Open Area Test Sight (OATS) according to [6].

For measurements on devices operating under 30 MHz an OATS should be used together with an inductive shielded antenna, which reads the H-field only. According to [6], the measurements are valid for both near field and far field situations. In this case, an OATS without a conductive ground plane is required. These types of test sights should also ideally be free of any buried metal objects such as pipes or other conductive material, which can affect the measurements [6].

4 Measurement setups

4.1 Field Strength Measurement

To verify that the systems do not violate the *EN 300 330* [6] regulations. A relative measurement is carried out.

As explained in Section 3.8, ETSI requires a shielded loop antenna for inductive measurements in the LF frequency ranges. An antenna, (*TELEC CT1*), is borrowed from SINTEF for this purpose. This is a shielded loop antenna whose main purpose is to measure unwanted magnetic noise from equipment for EMC regulations. It is capable of measuring magnetic fields in the frequency range 10 kHz - 150 kHz, which makes it suitable as the receiving end for a field strength measurement setup. The antenna has an impedance of 50 Ω so it can be connected to an instrument without any need for extra calibration.

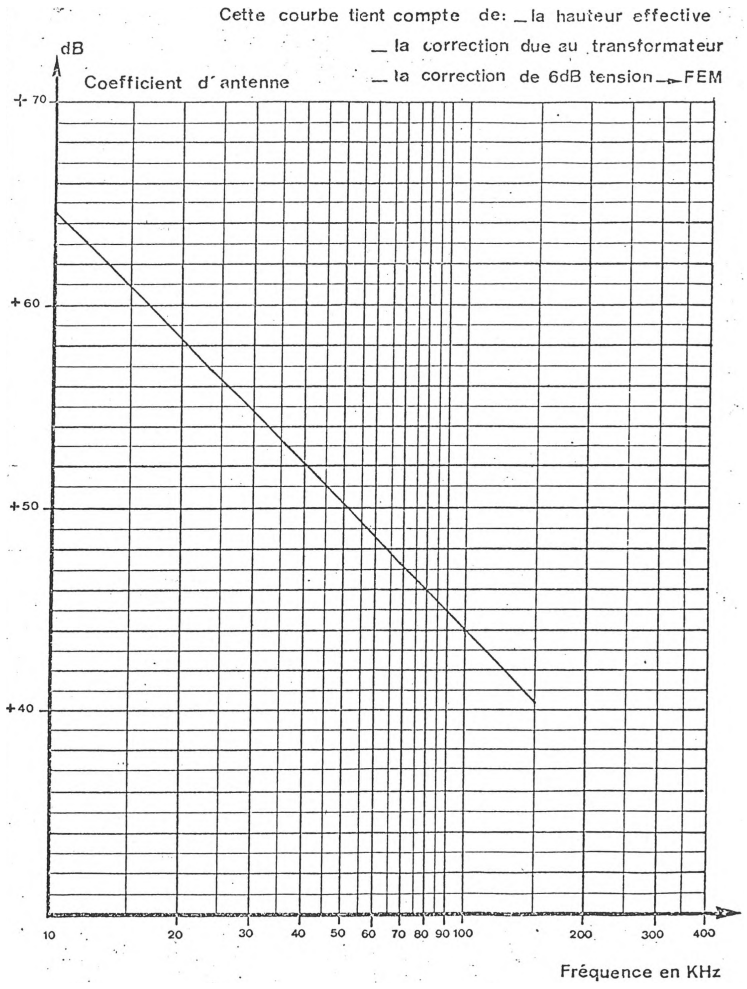

Figure 25: Antenna factor of the TELEC CT-1 for frequencies 10 kHz to 150 kHz [27]. Correction factor AF in this figure is for measurements in dBµV.

The correction factor AF of the antenna is frequency-dependent and is given by the curve in Figure 25. The value should be added using a decibel formula when measuring field strengths. As mentioned in Section 3.7, when measuring the magnetic field strength the free space impedance is required to convert the result into magnetic field strength. In dB terms, it can be written as

$$H_{meas} = V_{ant} + AF - Z_0, \tag{18}$$

where
H_{meas} Measured magnetic field strength $[\mathrm{dB\mu A/m}]$
V_{ant} Induced antenna voltage [dBµV]
Z_0 Free space impedance in decibel [dBΩ]
AF Antenna correction factor $[\mathrm{dBm^{-1}}]$.

The receiver that is used in the measurement setup is the *R&S Spectrum Rider FPH* spectrum analyzer. This is a handheld spectrum analyzer with a frequency specification of 5 kHz to 44 GHz. It is set to measure dBµV in the frequency range 130 kHz to 140 kHz with a resolution bandwidth of 300 Hz.

The RFID readers are placed at a 3 m distance from the H-field antenna, as that is the only possible configuration in the lab. The antennas on the readers are placed with the axial direction pointing in the axial direction of the H-field measurement antenna as this is the direction where the magnetic field propagates the furthest, accordingly to the interrogation zone as shown in Figure 23. As mentioned in Section 3.8 the 3 m distance measurement is not defined explicitly in the *EN 300 330 Standard*, so a conversion factor is required. This factor can either be added to 10 m limit value, to extrapolate the allowed field strength at 3 m. Or it can be subtracted from the measured field strength at 3 m, to extrapolate the measured field strength at the 10 m distance.

The conversion factor is denoted by ETSI as C_3 and is found using Figure 26.

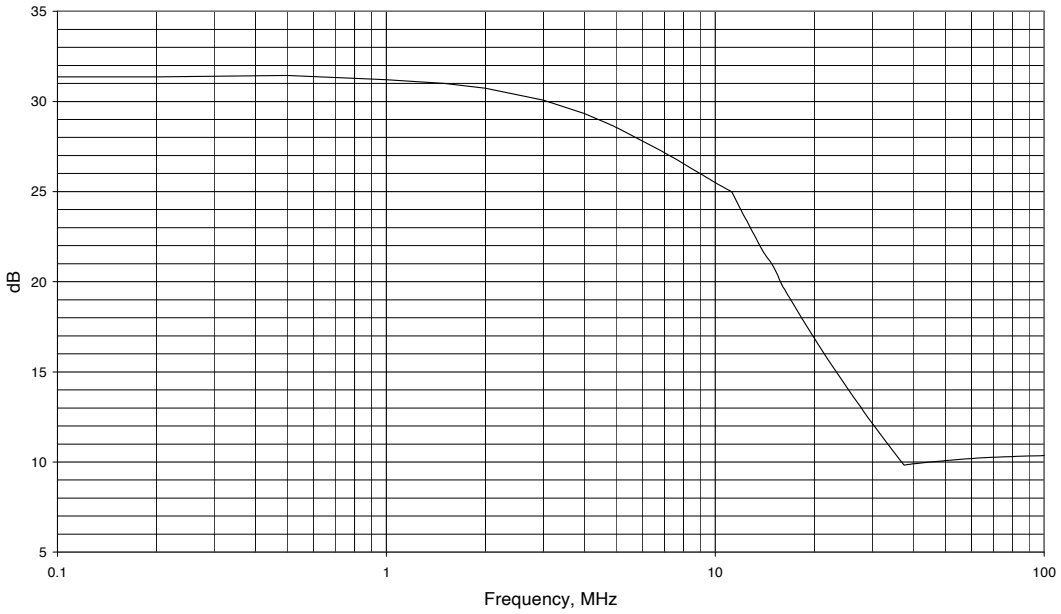

Figure 26: Conversion factor for measurements done at 3 m distance, versus frequency [6].

The H-field limit at 3 m is then determined by the following equation

$$H_{3\,\mathrm{m}} = H_{10\,\mathrm{m}} + C_3, \tag{19}$$

where
$H_{10\,\mathrm{m}}$ is the field strength limit in dBµA/m at 10 m
C_3 is the conversion factor found using Figure 26.

The measurement from spectrum analyzer is then plotted in MATLAB, and the measured peaks for each measurement is furthermore used for calculations. The calculations are also done in MATLAB, where both field strengths at 3 m and extrapolated to 10 m is calculated. Using Equation 18 for the measurement at 3 m distance, and re-writing Equation 19 with respect to $H_{10\,\mathrm{m}}$ for the extrapolated field strengths at 10 m.

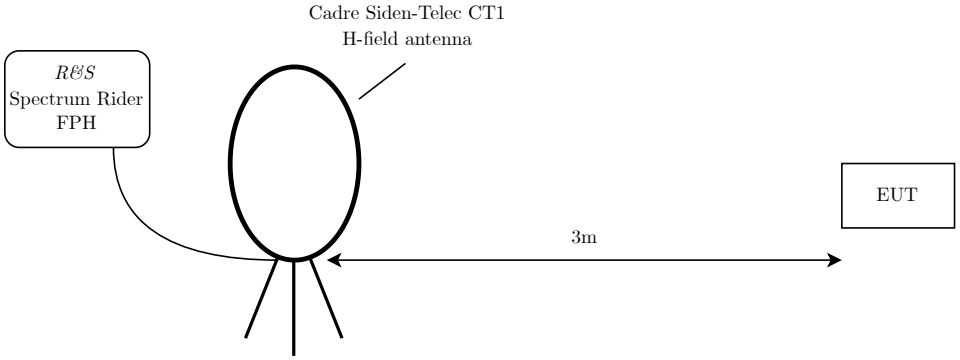

Figure 27: Measurement setup for measuring magnetic field strength generated by the readers.

4.2 Interrogation Zone Measurement

To measure the operational performance of each designed system, the interrogation zone is measured. This is done by placing the EUT in a fixed location and moving the transponders in the vicinity around the reader until a valid detection is achieved. Using a fixed angle towards the axial direction of the reader's antenna. The measurement is then done by noting the range for each detection by the EUT, in φ-sectors of 5°s in a circle around the EUTs ferrite antenna.

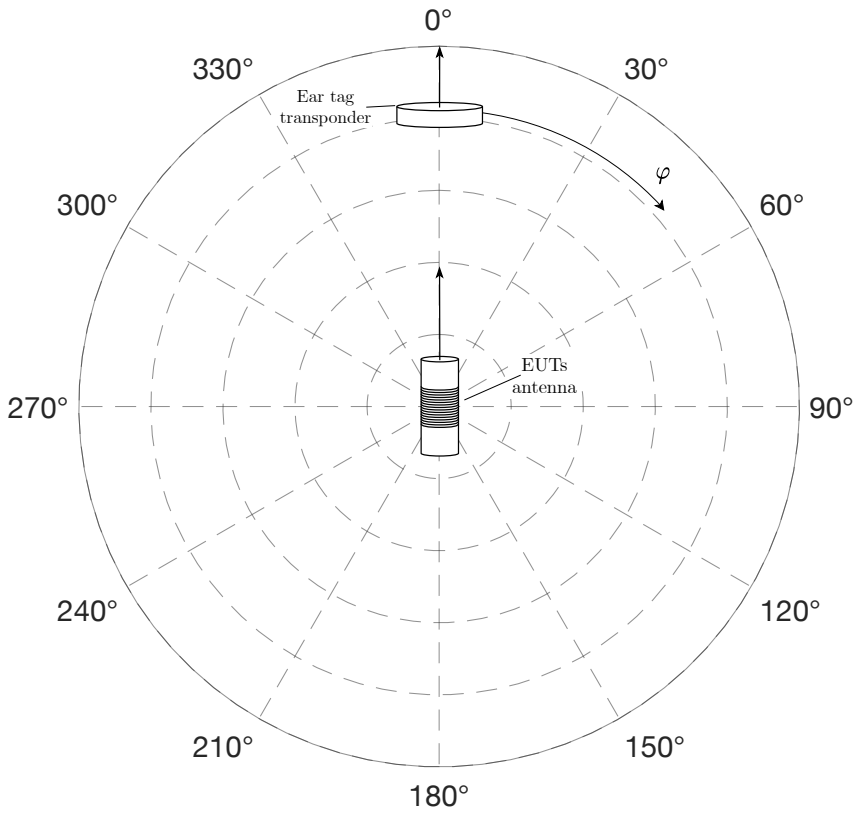

(a) Movement of transponder during tests.

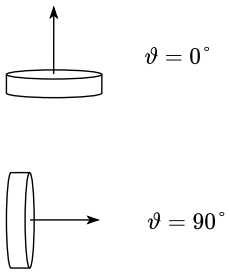

(b) Orientation of transponder during tests.

Figure 28: Interrogation Zone Measurement.
φ is the direction where the transponder is moved in relation to the EUT during the tests.
ϑ is the displacement angle for the transponder in relation to the EUTs antenna.

The test is done twice for each device, one where the transponders displacement angle was fixed at $\vartheta = 0°$ in relation to the axis of the EUTs ferrite antenna. Another one with the transponders displacement angle fixed at $\vartheta = 90°$ in relation to the axis of the EUTs ferrite antenna. Figure 28b, illustrates the two orientations the transponder has in the tests. Figure 28a illustrates the orientation of the EUTs ferrite antenna in relation to the transponder.

As the software currently only does decoding, an *Atmel ATA2270-EK2* development board is connected to the FDX-B reader to determine valid detections. For the HDX reader, determining valid detections is done by monitoring the SCIO data line using an oscilloscope, as this only produces a data stream when a transponder is successfully read.

5 Design and Implementation

5.1 FDX-B Reader/basestation

The following chapter explains the circuit from the application note [28], which is implemented within the project.

The FDX-B reader is based on the *EM4095* as the radio front-end. This ASIC handles most of the key functions which are needed in an LF RFID reader. Such as transmitting a signal which can power the transponder, receiving a response signal from the transponder which is not superimposed by the transmission signal, and finally producing a readable output for a microcontroller or similar.

The implemented system in this project bypasses many of the built-in functionalities in the *EM4095*, to optimize for read range. For transmission, firstly the internal antenna driver is only used in a single-ended configuration, instead of the normal differential configuration. It is then used in an external power stage, which is capable of driving the antenna at a higher power level. In addition to the modification on the transmission side, the receiver part of the system is also slightly modified from the normal operation of the *EM4095*, as there is an external demodulator that is more sensitive and can handle higher voltage and current than what is internal in the ASIC.

The block diagram in Figure 29 illustrates the most important system blocks for the implemented FDX-B reader.

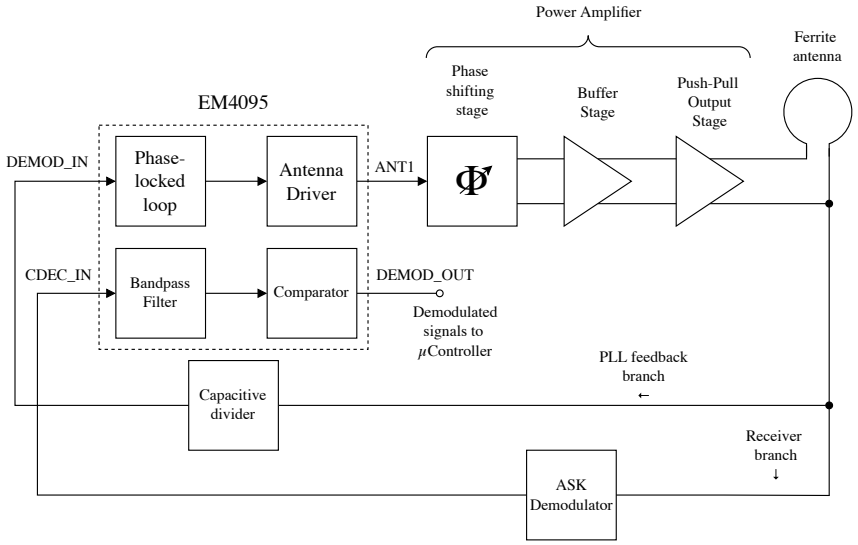

Figure 29: Functional block diagram of implemented FDX-B reader. Blocks within the dashed square are internal parts of the *EM4095* ASIC, blocks outside are discrete elements.

5.1.1 Power amplifier

The power amplifier boosts the output signal beyond what the *EM4095* ASIC is capable to produce on its own. The *EM4095*s internal antenna driver can handle currents up to 250 mA while the power amplifier is said to be able to handle currents up to 2 A. This means that the reader can produce a magnetic field strong enough to activate transponders at a greater distance.

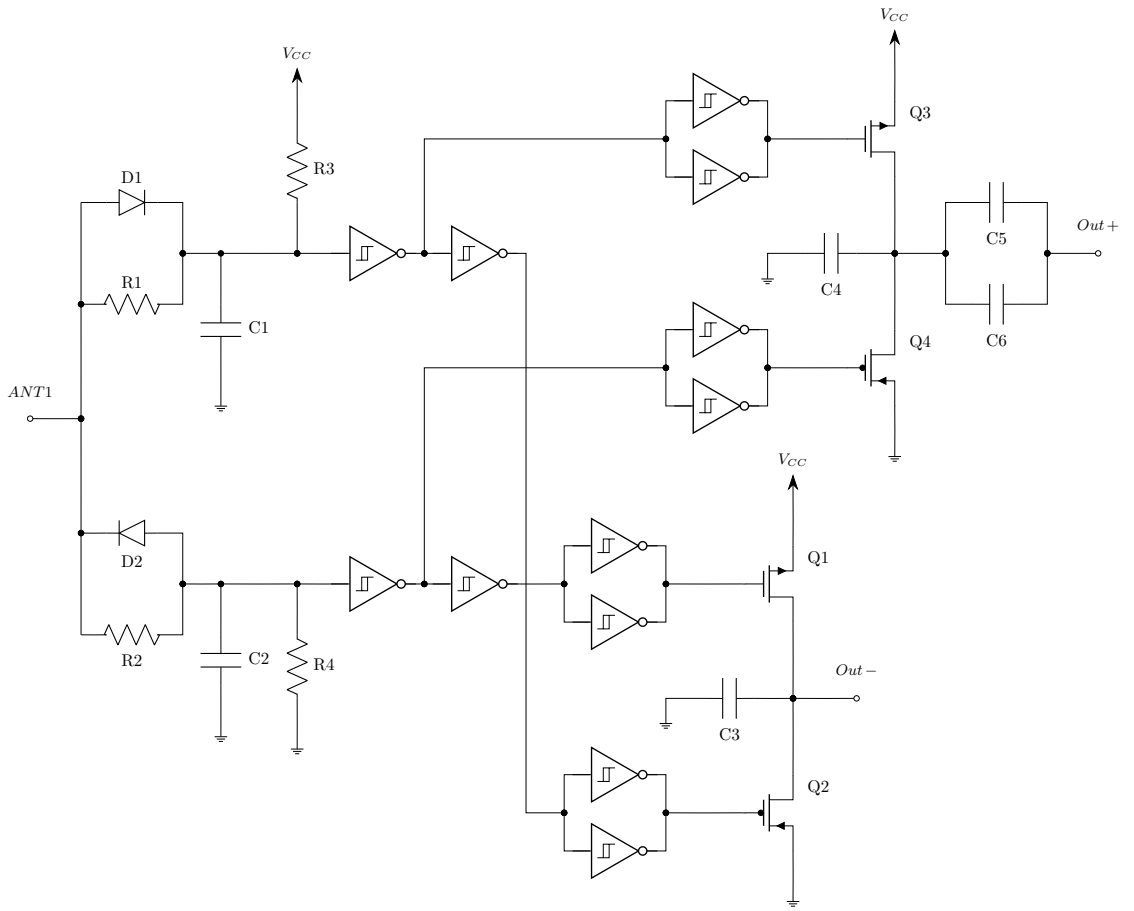

Figure 30: Power amplifier architecture.

The power amplifier or driver circuit is composed of essentially three stages, a phase-shifting stage, a driving stage, and an output stage. The entire schematic for the power amplifier architecture is shown with Figure 30.

The first stage of this amplifier is the phase-shifting stage. This stage clamps the sinusoidal produced by the *ANT1* output from the *EM4095* with a simple diode-based voltage clamp. This makes the voltage swing between different amplitudes for the top and bottom branches. After the voltage clamp, the voltages are fed into the first Schmidt trigger ports, which essentially rectifies the sinusoidal voltage to a square voltage, for both branches. As the sinusoidal voltage is clamped to different amplitudes, the Schmidt triggers will produce a differential square voltage that has a different duty cycle. These voltages are phase-shifted from each other and fed into another set of Schmidt triggers, which inverts both branches. This then creates four parallel branches which drives can drive the following stages.

The voltages are then fed into a set of parallel coupled Schmidt triggers which composes the driving stage. These networks ensure fast switching on the output CMOS stage and are connected in parallel to reduce the resistance going into the gates of the CMOS stage. After this, the voltages are fed into the CMOS pairs which make up the final output stage.

This output stage is composed of a differential push-pull CMOS pair. The output stages transistors are chosen accordingly to [28], and to have an R_{DSon} able to drive antenna currents up to 2 A. As this is a relatively small on-resistance it is necessary to have the fast phase-shifted signal to switch the output stage in a break-before-make manner. This avoids having both PMOS and NMOS transistors on at the same time which could cause a large cross current.

Lastly, the two capacitors $C5$ and $C6$ make up the capacitive part of the resonant circuit, which is connected to the antenna.

5.1.2 External demodulator

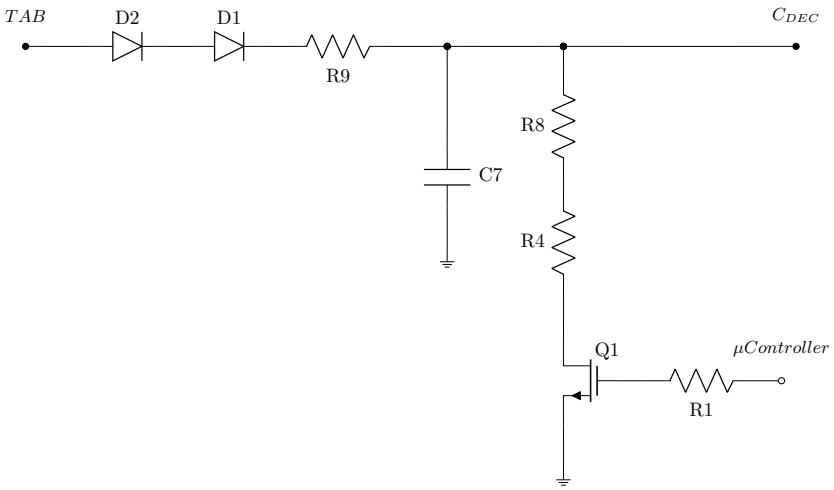

Figure 31: External demodulator.

The second measure to increase range is by using a demodulator with higher sensitivity than what is present in the internal demodulator in the *EM4095*. This is done by not using the *CDEC_OUT* pin, and instead constructing a discrete demodulation circuit as shown in Figure 31. The demodulator is constructed using two diodes to compensate for any high voltage present at the antenna terminal. A series resistor is also present to limit the current in this branch. After these elements there is a *RC* circuit which is a common demodulator topology, however the transistor $Q1$ can enable or disable the resistors $R8$ and $R4$. The transistor is normally closed, so to disable the resistive branch, one would have to bias the transistor.

5.2 Layout

Layout was done accordingly to [28], where the main aspects to follow is separating the analog reception part from the "digital" transmitter part. In addition to this the layout of the circuit includes a net-tie and another antenna port for the purpose of testing whether a dual antenna configuration could benefit the system performance. The layout is included in the Appendix B.

5.2.1 Firmware

As the *EM4095* only demodulates the transponder response, a software is written for the *ATmega328P* microprocessor, to decode and process the response into readable information.

As the demodulated signal is still encoded, it is necessary to decode this signal to receive the correct telegram as presented in Section 3.3.3. The demodulated signal is simply a square wave with different pulse lengths, and to sample this an *input capture interrupt* is used. The reason for using an input capture is that it can accurately measure the time between rising edges of square signals. This creates essentially three different time intervals for decoding. A long interval when sequential ("1")s are received, a medium interval when a ("1") is received after a ("0") or vise-versa, and lastly a short interval when ("0")s is received. This is illustrated in Figure 32.

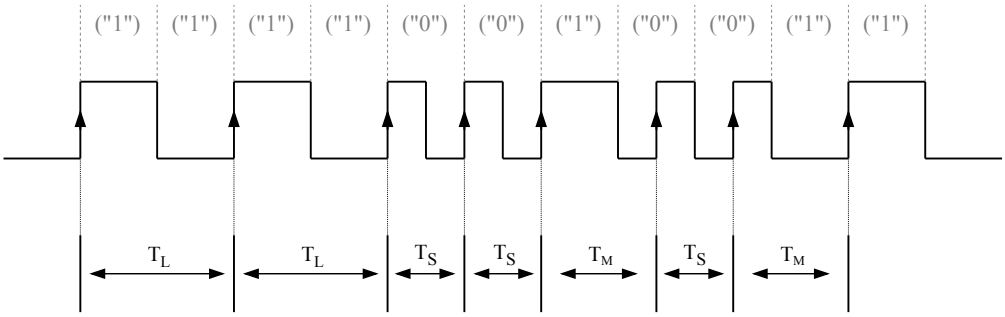

Figure 32: Implemented decoding principle: T_L timing interval corresponds to ("11"), T_M timing interval corresponds to either ("1") or ("01"), T_S timing interval corresponds to ("0").

The decoder simply decodes by saying that a time interval equivalent to the T_L is two sequential ("1")s. A short interval equivalent to T_S is decoded as a single ("0"). Finally the time interval equivalent to T_M is decoded using an extra parameter which acts as a remainder. When a T_M is detected for the first time it is decoded as a single ("1"), and the remainder is set. The next time a T_M is detected it is decoded to be a sequential ("0") and ("1"), and the remainder is reset. This alternates throughout the decoding process. The source code for this decoder is included in Appendix C.

5.3 HDX Reader/basestation

The HDX reader is implemented using the *TMS3705* base station ASIC from Texas Instruments. This ASIC serves as an analog front-end as well as a decision device that demodulates and performs decisions on an incoming FSK modulated RF signal. The output of this ASIC is an Non-Return-to-Zero (NRZ) encoded serial data stream with a frequency 15.625 kBaud/s. Figure 33 summarizes the most important system blocks for the *TMS3705*.

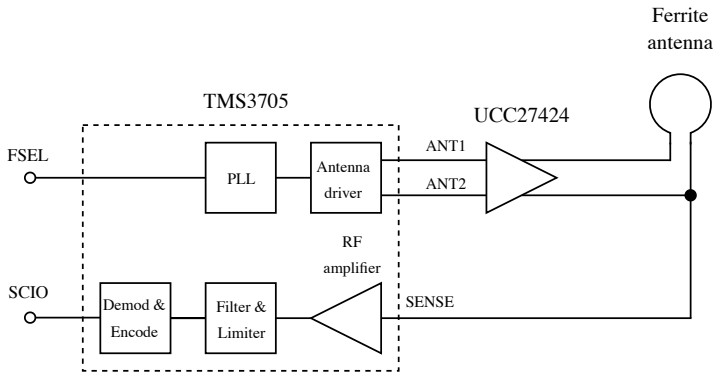

Figure 33: The most important system blocks in the HDX reader.

5.3.1 Power amplifier

Together with the *TMS3705*, an external gain stage is added to maximize read range, and the *UCC27424* full-bridge driver is used as the gain stage. This is chosen based on the application note [29] and includes differential input and output. This allows using both antenna outputs from the *TMS3705*, which leads to a less complex gain circuit.

5.3.2 Receiver

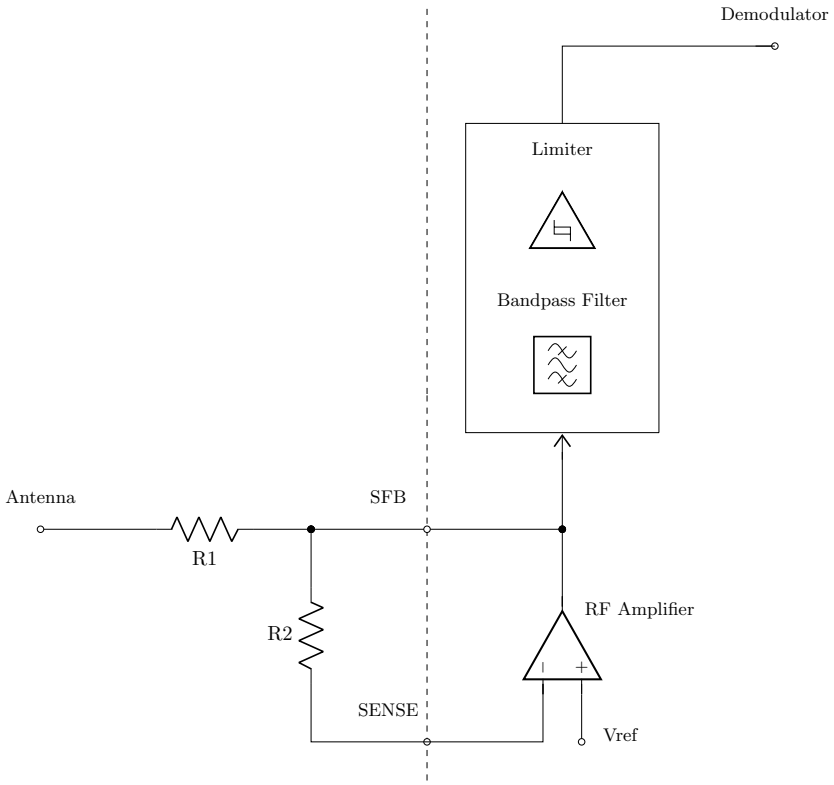

Figure 34: TMS3705 reception circuitry, external and internal parts are separated by the dashed line.

The internal receiver of the *TMS3705* is set up using external components. The pins *SFB* and *SENSE* is connected to the inverting input and the output of an internal RF amplifier, respectively. The positive input of this internal RF amplifier is an internal voltage reference set up by the ASIC itself. This creates an inverting op-amp configuration where the gain is set by the resistors *R1* and *R2*. This gain is described by the following equation

$$G_{Rx} = \frac{R2}{R1}. \tag{20}$$

5.4 Layout

The HDX base station PCB layout is done by following the principle of the FDX-B reader, splitting the transmitter part and receiver part into each sector of the PCB. The HDX circuit requires a 12 V and a 5 V rail, so an additional power regulation part is added to the circuit. The receiver part is located on the left side, the transmission part is in the centre and the regulation part is on the right side of the layout. The layout is included in Appendix E, where both the topside and bottom side of the PCB can be viewed.

5.4.1 Firmware

The *TMS3705* produces a serial output with one start bit and one stop bit for each byte when a transponder has been successfully read. However, as this output is sent at the rather unusual 15.625 kBaud/s it cannot be read out using a simple UART interface or alike. Due to this, a software is developed for the *ATmega328P* using a pin change interrupt which initiates a sampling procedure

on the SCIO line. The sampling procedure is triggered after 3032 ms which is in accordance with the timing in the data sheet [11]. The sampling procedure samples the SCIO line at every 64 µs which will be the center of each bit period. The *TMS3705* encodes the data using an NRZ scheme, which means that a ("1") is interpreted as a ("1"), and a ("0") is a ("0"). However, the output is inverted so it has to be inverted to be translated into decimal data.

5.5 Antennas

The ferrite antennas are designed using ferrite rods from *Fair-Rite Corp.*. The rod material is the 78 material which is a (MnZn) based ferrite material optimized for low loss inductive applications up to 500 kHz.

The permeability of the 78 material is supplied from [30] which is plotted in Figure 35. The f_o is marked with a vertical line at 134.2 kHz, taking the real and complex values of the permeability,(μ), at this point, $\Re(\mu) = \mu' = 2108.6$ and $\Im(\mu) = \mu'' = 15.383$, and using them in Equation 7 produces loss tangent $tan(\delta) \approx 7.295 \cdot 10^{-3}$ at 134.2 kHz.

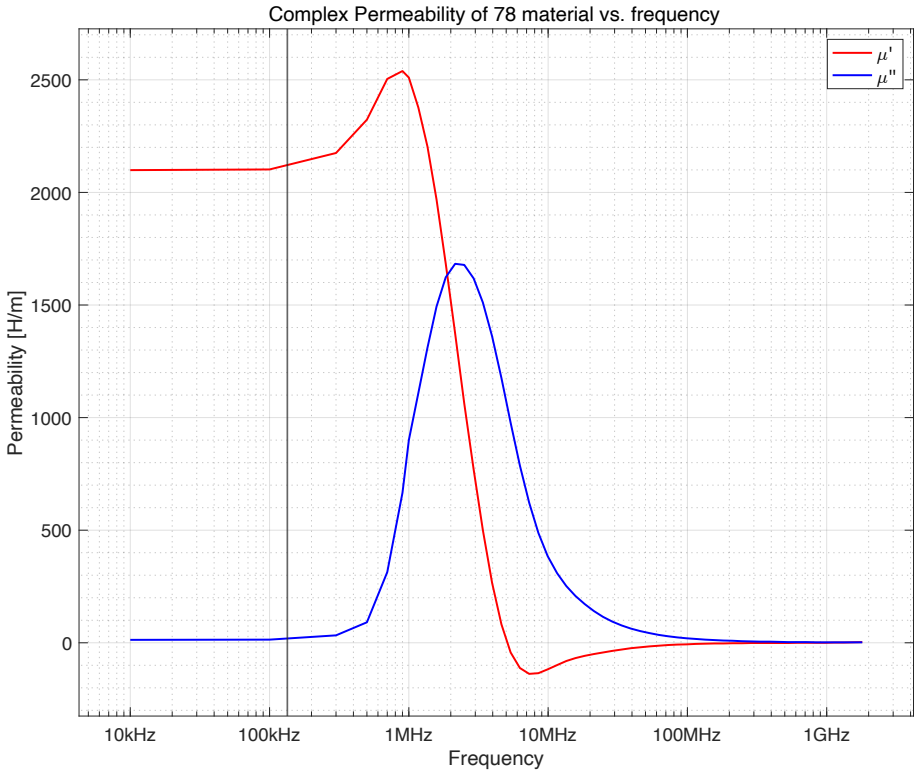

Figure 35: Real component $\Re(\mu) = \mu'$ & Complex component $\Im(\mu) = \mu''$ of the permeability of the 78 material plotted against frequency, with data from [30].

The antennas are designed to resonate at 134.2 kHz with a resonance capacitance of 6.6 nF. Using the scripts bundled with [23]. Inputting the mechanical dimensions from the ferrite rods produces the inductance factor (A_L). If Equation 8 is rearranged the number of turns n can be found for a desired inductance L

$$n = \sqrt{\frac{L}{A_L}}. \tag{21}$$

Three different antennas with different mechanical sizes are crafted using the script from [23] to find the inductance factor, and the number of turns were determined from Equation 21.

6 Results

6.1 Antenna Design

The antennas are tuned to resonate at 134.2 kHz, with each circuit's resonance capacitor network having a capacitance, $C = 6.6\,\text{nF}$. The required antenna inductance is then found by rewriting Equation 11 with respect to L

$$L = \frac{1}{4\pi^2 \cdot (134.2\,\text{kHz})^2 \cdot 6.6\,\text{nF}} \approx 213\,\mu\text{H}.$$

Determining the required number of turns to achieve the desired inductance is done by firstly using the MATLAB script. From this, the inductance factor (A_L) is obtained and then rewriting Equation 21 with respect to the number of turns (n). For the smallest ferrite antenna, the estimated number of turns becomes

$$n = \sqrt{\frac{213\,\mu\text{H}}{40.412\,\text{nH}/n^2}} \approx 72.6 = 73\,turns.$$

This process is done on each of the three different antennas. There is some overshoot/undershoot from the MATLAB estimation, which is corrected by unwinding/winding some of the turns. After winding the required number of turns, the antennas can be measured using an LCR meter. A *BK Precision 895 bench LCR meter* together with a *BK Precision TL89 1K Test Fixture* probe, was used to measure the designed antennas.

Table 2 shows the mechanical dimensions, estimated inductance, measured inductance, and final inductance after correction, for all the three antennas designed.

Table 2: Mechanical dimensions, estimations initial measurements and corrected measurements for each antenna designed.

Parameters \ Rod label	Short	Medium	Long
Rod length (ℓ_f)	38.10 mm	45.00 mm	70.00 mm
Rod diameter (d_f)	9.45 mm	8.00 mm	9.50 mm
Coil length (ℓ_c)	28.78 mm	32.35 mm	21.18 mm
Relative permeability (μ_L)	1.69 H/m	1.70 H/m	2.44 H/m
Inductance factor (A_L)	$4.04 \cdot 10^{-8}\,\text{H}/n^2$	$4.05 \cdot 10^{-8}\,\text{H}/n^2$	$7.89 \cdot 10^{-8}\,\text{H}/n^2$
Estimated inductance (L_e)	215.35 µH	215.58 µH	213.44 µH
Estimated number of turns (n_e)	73	73	52
Measured inductance (L_i)	224.45 µH	222.36 µH	209.16 µH
Measured inductance after correction (L_c)	213.56 µH	212.42 µH	214.26 µH
Corrected number of turns (n_c)	70	69	53

6.2 FDX-B Performance

Using the setup described in Section 4.2, placing the EUTs antenna in a fixed location while rotating the transponder in the vicinity around the reader antenna (φ), while maintaining a fixed displacement angle ($\vartheta = 0$). The interrogation zone which describes the performance of the system is measured. Figure 36 shows the interrogation zone for the FDX-B reader, with both transponder configurations.

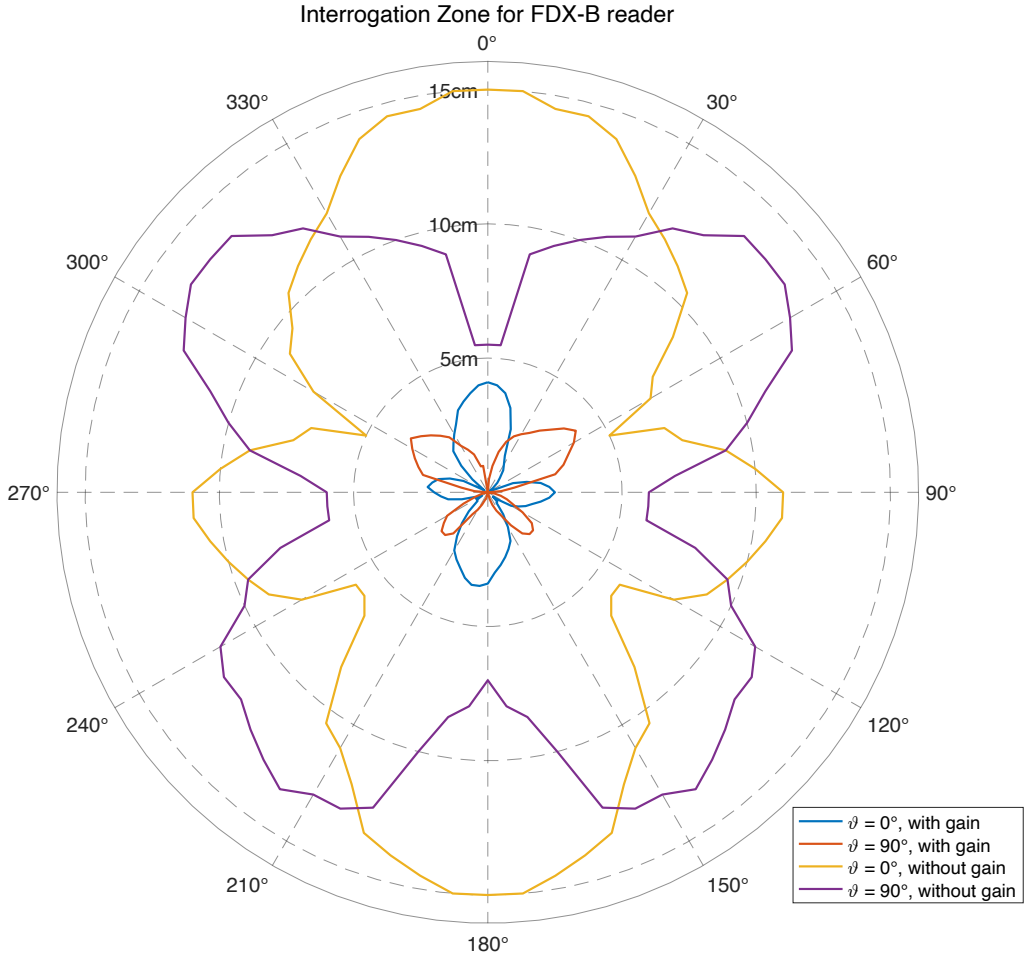

Figure 36: Measured interrogation zone of FDX-B reader

Figure 36 shows the interrogation zone with and without the external gain stage. The peak range when $\vartheta = 0°$ is in the direction where $\varphi = 0°$ and 180°. This means that the greatest range is achieved when the transponder and reader's antenna axis is in the same direction. When the transponder is perpendicular to the reader's antenna axis, the greatest distance is achieved at approximately $\varphi = 50°, 140°, 230°$, and 320°. Due to the limited distance achieved with the gain stage, another measurement is done with modifications to the circuit[1]. For the test done with the gain stage, the peak range when $\vartheta = 0°$ is approximately 4.1 cm, and 4 cm when $\vartheta = 90°$. When the gain stage is bypassed and demodulator modified, the peak range is about 15 cm when $\vartheta = 0°$ and around 13.5 cm when $\vartheta = 90°$. In the measurements, the medium length antenna is used due to its spectrum measurement, which is shown later in Figure 39.

[1]The circuits external gain stage is bypassed. In addition to this, the external demodulator is reduced to a single diode and just the *RC* low-pass filter, without the series resistor.

6.3 HDX Performance

The same is done for the HDX reader, using the same measurement configurations for both reader antenna and transponder.

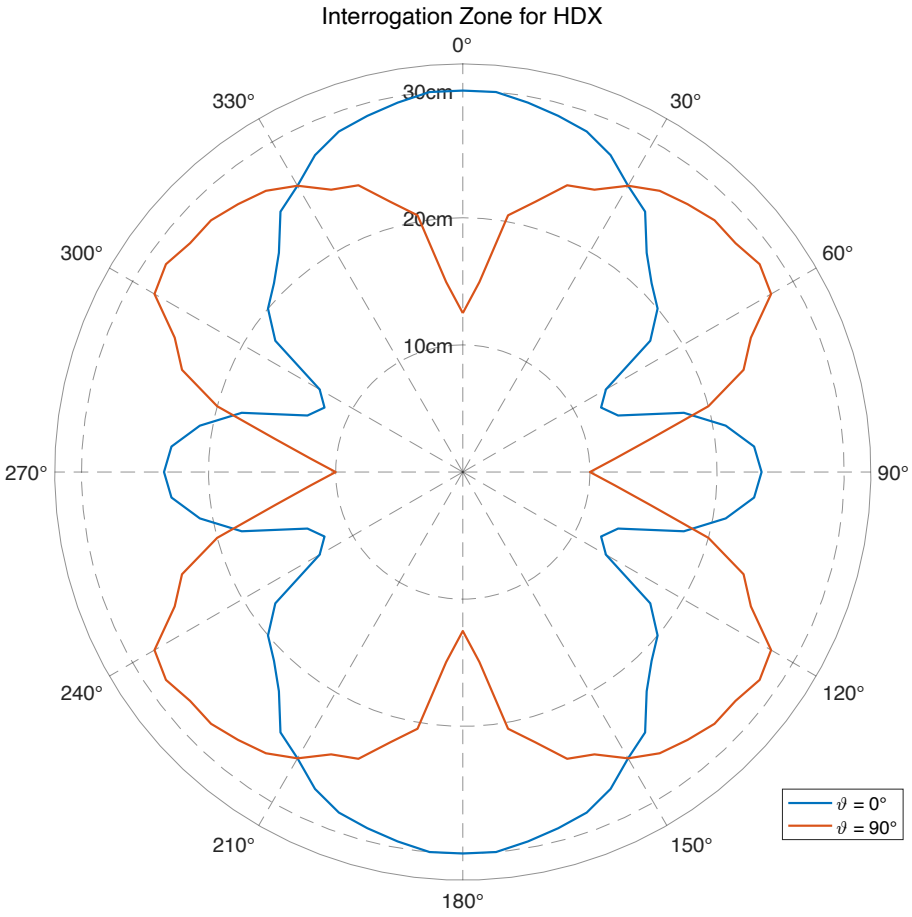

Figure 37: Measured Interrogation zone for the HDX transponder.

From Figure 37 shows the measured interrogation zone. Measured detection peaks for transponder angled $\vartheta = 0°$, with 30 cm at $\varphi = 0°$and $\varphi = 180°$. 23.5 cm at $\varphi = 90°$and $\varphi = 270°$. Measured detection peaks for transponder angled $\vartheta = 90°$, with 28.5 cm at $\varphi = 55°$, $125°$, $235°$and $305°$.

This measurement are using the longest ferrite antenna due to its performance in the spectrum measurement which is shown later in Figure 40.

6.4 Field Measurements

The setup from Section 4.1 measures the induced voltage on the measurement antenna in dBµV. Figure 38 shows a picture of the HDX reader's transmitted field being measured.

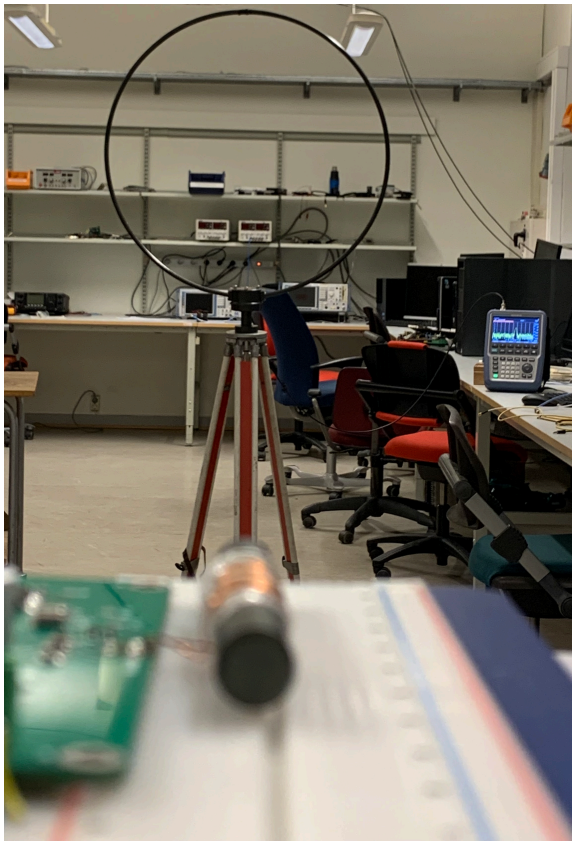

Figure 38: Field measurement of the HDX reader, measurement antenna and *R & S* spectrum analyzer in the background.

The RMS voltage of the antennas on each device is also measured using a multimeter, for the HDX the RMS voltage is approximately 140 V across the antenna terminals. For the FDX-B reader, the RMS voltage is approximately 283 V across the antenna terminals.

For the FDX-B reader, measuring with all three designed antennas yields the measurement presented in Figure 39.

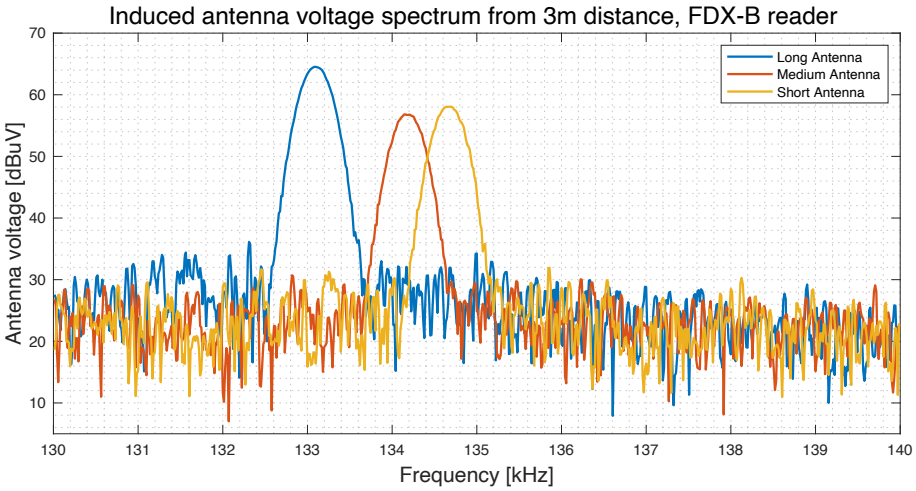

Figure 39: Measured spectrum, FDX-B reader.

Using MATLAB, the field strengths for all six measurements are calculated at the measurement distance of 3 m. As well as extrapolated to a distance of 10 m. These calculations are done by rearranging the equations from Section 4.1, Equation 18 for field strength measurements at 3 m distance, and Equation 19 for the extrapolated results. For the long antenna together with the FDX-B reader, the field strength at 3 m then becomes

$$H_{3\,\mathrm{m}} = 64.5\,\mathrm{dB\mu V} + 41\,\mathrm{dBm^{-1}} - 51.5\,\mathrm{dB\Omega} = 54\,\mathrm{dB\mu A/m},$$

and extrapolated to 10 m

$$H_{10\,\mathrm{m}} = 54\,\mathrm{dB\mu A/m} - 31.2dB = 22.8\,\mathrm{dB\mu A/m}.$$

The measured field strengths done at 3 m, as well as the extrapolated field strengths at 10 m for the FDX-B reader is listed in Table 3.

Table 3: Measured magnetic field strengths $H_{3\,\mathrm{m}}$ and extrapolated field strengths $H_{10\,\mathrm{m}}$, for the FDX-B for all three different designed antennas.

Field-Strength \ **Rod label**	**Short**	**Medium**	**Long**
$H_{3\,\mathrm{m}}$	47.5 dBµA/m	46.3 dBµA/m	54.0 dBµA/m
$H_{10\,\mathrm{m}}$	16.3 dBµA/m	15.1 dBµA/m	22.8 dBµA/m

The same is done for the HDX reader, measuring with each designed antenna. This yields the measurement in Figure 40.

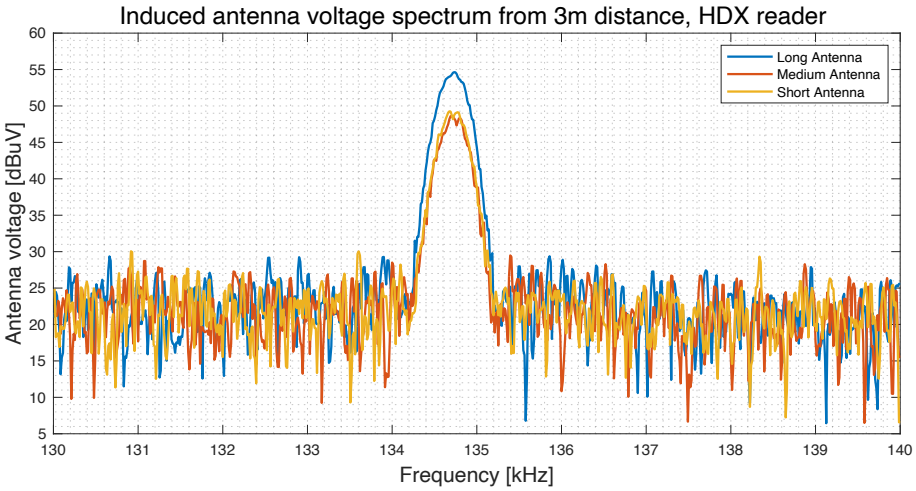

Figure 40: Measured spectrum, HDX reader.

Also calculating the measured magnetic field strengths at 3 m and the extrapolated field strengths at 10 m for the measurement in Figure 40. This is listed in Table 4.

Table 4: Measured magnetic field strengths $H_{3\,\mathrm{m}}$ and extrapolated field strengths $H_{10\,\mathrm{m}}$, for the HDX for all three different designed antennas.

Field-Strength \ **Rod label**	**Short**	**Medium**	**Long**
$H_{3\,\mathrm{m}}$	38.7 dBµA/m	38.1 dBµA/m	44.1 dBµA/m
$H_{10\,\mathrm{m}}$	7.5 dBµA/m	6.9 dBµA/m	12.9 dBµA/m

7 Discussion

7.1 Antennas

The antennas designed show that it is possible to design ferrite loop antennas with a pretty high level of accuracy, just by using the scripts from [23]. As there is no such thing as a half-turn when it comes to inductors, there is a limitation in the resolution of inductance achievable for these antennas. This means that more care, than what is done with the currently designed circuits, should be spent designing the resonance networks. By using more capacitors, a higher level of accuracy can be reached by setting the correct resonance for the antenna circuits.

The 78 material seems to be a very good material for these types of applications, looking at Figure 35 from Section 5.5 it is shown that the real part of the permeability of the 78 material, $\Re(\mu)$, is much larger than the complex part, $\Im(\mu)$. This means that the loss tangent is quite low, $7.3 \cdot 10^{-3}$ at 134.2 kHz. This means that at this frequency, most of the current in the antenna will be active current as appose to reactive.

The antennas crafted show that it is possible to achieve good performance while maintaining limited physical dimensions. This shows that it is not necessarily the physical size of the reader's antenna which limits the range.

7.2 FDX-B Reader

The FDX-B reader is built up using a relatively comprehensive gain stage, with many external components. This gain stage generates a strong magnetic field, and as the field measurements in Table 3 show, the highest using the longest antenna. The field of the longest antenna is almost 10 dB higher than the other antennas tested, however at a slightly lower frequency than 134.2 kHz. In comparison to medium length antenna which runs at exactly 134.2 kHz, as shown by Figure 39. All these field strengths are within the regulations given by ETSI of 66 dBµA/m, with the highest measured peak of 54.0 dBµA/m at 3 m. So all the measured field strengths at 3 m is lower than the regulatory limit at 10 m, meaning that the regulation seems generous in terms of what is allowed for transmission. The demodulator is designed to withstand the increased signal level created with the implemented gain. Using two series diodes, and a series resistor limits the powerful transmit signal from burning the receiver input of the *EM4095* ASIC.

Regardless of these external networks the range is still quite limited. This is most likely caused by the external gain stage gaining the signal to a level that superimposes the reception part of the reader. Modifying the circuit to bypass the gain stage and reducing the demodulation stage to a single diode and shorting the series resistor increases the range by a factor of 3. As the interrogation measurement in Figure 36 show, the range is increased from 5 cm to 15 cm. This implies that the main limiting factor of this system is the sensitivity of the reception, and not the standard signal level produced by the Application Specific Integrated Circuit (ASIC), as this range is achieved with external demodulation and without external gain. The diode used has a forward threshold voltage of 0.6V which is a relatively high threshold for weaker reception signals. Replacing this diode for a schottky diode with a lower threshold could potentially increase this range even further. Lastly substituting the gain stage to a less comprehensive gain stage which just slightly raises the output signal level without superimposing the reception, could also increase the range.

The software developed for the *ATmega328P* microprocessor is able to measure the pulses produced by the *EM4095*, but has to be developed further to actually produce a readable output. Nevertheless, the system's performance is confirmed using the *Atmel ATA2270-EK2* development board.

7.3 HDX Reader

The HDX reader is simpler in construction and uses fewer system blocks in comparison with the FDX-B reader. Its gain stage is simply a full-bridge driver, which amplifies both rails supplied by the internal antenna driver. The reader also measures out to have a transmitted field strength that is below the limit, as Table 4 shows. These measurements also show that regardless of the antenna, the circuit operates at a frequency of 134.7kHz which is a bit above the operational frequency of LF RFID at 134.2 kHz. A closer inspection of the field measurements shows that 134.2 kHz is in fact located in the noise floor of the measurement. Nevertheless, the reader shows great results given that it has a peak read range of 30 cm which is very decent given the size of the antenna. If the peak operational frequency is moved to 134.2 kHz it could likely increase the range even further than what is currently measured. The ASIC allows for digitally controlling the operational frequency, but the closest available frequency which can be set is the default frequency. Another solution to possibly achieve greater range is to reduce the Q value of the resonant circuit as according to Figure 19 this would give the system a wider bandwidth which might cover the operational frequency. This is however not a possibility given the current circuit layout. The reception part of the circuit is constructed using an internal operational amplifier. The gain of this amplifier is set by external components. No modification was done to this gain, however modifying this could potentially increase the range, more. Nevertheless, the read range of the reader is still quite decent and might be satisfactory for an automatic configuration as described in Section 2.

7.4 Measurements

The field measurements done, are relatively precise. The equipment is accurate, but the test sight has some short comings. Ideally the test sight should be a proper OATS as described in Section 3.8. Being able to mount the EUTs antennas on an antenna mast as described in Section 3.8, would allow for easier and more accurate peak detection. This would ensure that the absolute strongest field strengths produced is measured. The current setup is also located in a relatively noisy environment, as there are a lot of other electrical equipment located in the lab, some of which can be seen in Figure 38. Not just accurate measurement equipment with high EMI specifications, but also equipment like switch mode power supplies for computers and HVAC systems. The test sight is also not clear of conductive elements like pipes and other infrastructural conductive object, which a test sight for these types of measurements should be clear of as described in Section 3.8.

The measurement antenna is quite old and is rarely used, so some deviations in the antenna parameters is not unlikely. Additionally the correction factor is read out manually, which is not that accurate. Especially given the logarithmic frequency axis of the correction factor. Interpolating this value using the clearest data points, would decrease the level of uncertainty associated with these measurements.

The interrogation zone measurements is done by hand using a protractor and a ruler for measuring the φ angle and the range from the readers antenna, respectively. This is not a very accurate way of measuring, but gives a good feel of how the systems perform, and the measurements creates similar results to the illustrations presented in Figure 23. Ideally these tests should be done using an antenna turret or similar, where the φ angle is measured more accurately, and the detection range at these angles is measured using a distance sensor rather than a ruler. Nevertheless the measurements gives a good feel of which configurations of reader and tag which yields the best read range.

8 Conclusion

Throughout this project, two long-distance LF RFID systems are successfully implemented and verified using mostly available tools. The theoretical background describes how the systems are fundamentally built up and how they function.

The results show that an automatic system is plausible, but this has yet to be tested in the field on actual livestock animals. As aspects such as the transponder displacement angle, ϑ, greatly influences the interrogation zone of the systems, antenna mounting considerations has to be taken into account for this to function. The HDX reader achieves a peak read range of 30 cm, which is very promising given that the system operates at a slightly higher frequency (134.7 kHz) rather than the operational frequency of the transponders of 134.2 kHz. The HDX reader also has a narrow bandwidth, so a bandwidth increase could potentially increase this read range. Additionally maximizing the area of an air-loop antenna, given the cross-sectional area of the Nofence collar could potentially achieve greater ranges than what is achievable using a relatively small ferrite core antenna, as used within the project.

The FDX-B system shows quite limited performance using the originally designed circuit. The modifications done improves the performance, yielding approximately a 3 times increase in range, going from 5 cm to 15 cm. This shows that the original circuits gain stage most likely superimposes the reception, as the transmitted downlink has a way higher field strength compared to the transponders uplink. Further optimization of the read range could potentially be achieved if a less comprehensive gain stage is implemented, such as the full-bridge driver used for the reader. Additionally, care should be taken to ensure a sufficient amount of isolation between the transmitter and receiver stage, so one does not have to use series resistors in the reception stage.

The field measurements show that both circuits are most likely operating in accordance with *EN 330 300*, but it cannot be said certain without an absolute measurement, which has to be done in accordance with the requirements explained in Section 3.8.

The current state of the software only does decoding, and prints decoded bits to an UART terminal. To ensure proper functionality, the decoded symbols should be processed further to supply the identification number and country identifier over UART or similar. Nevertheless, the performance of the systems is measured using, a development board on the FDX-B system, and an oscilloscope on the HDX system

The result of the explored configurations within this project shows that an automatic system is plausible. While maintaining limited physical dimensions and without violating regulations. The systems are more complex to implement than just using the ASICs without any desired range requirement. Additionally, the performance in a configuration like the wearable GNSS collar, as illustrated in Figure 1 in Section 2 has yet to be tested and verified, as the displacement angle ϑ greatly affects the performance of systems.

9 Further Work

Firstly the software has to be developed further, so it processes the samples into a readable format, as appose to just doing the decoding. Additionally, the systems can likely be tuned to reach better ranges, if the range is a desired metric of a system. As mentioned, there is most likely more potential in either frequency tuning in the HDX system, or gain and reception tuning for the FDX-B system. On the FDX-B system, one should also look into the isolation between the reception branch and the transmit branch, so that reception can avoid any sensitivity limiting factors like series resistors.

Other aspects such as FSK to ASK conversion should also be looked into, as using relatively few system blocks can potentially give the FDX-B reader the ability to reading both protocols. As mentioned in Section 3.3.5, the HDX protocol modulates binary data as 16 cycles for each frequency. The decoding required in to interpret the HDX data can then simply be a frequency counter, counting 16 cycles at each frequency. This means that if an FSK to ASK conversion could be done reliably, producing a square wave output with different frequencies, it could likely be decoded into a readable format. Which could make one reader able to interpret both protocols used with LF RFID.

Other use cases than the automatic detection of individual animals for IoT products for these systems, can be animal transportation. If a loop antenna is constructed around the entrance of an animal transportation truck, individual animals can be detected while entering the transportation truck. This could potentially give meat producers and farmers an extra level of accuracy, as appose to just using pen and paper for counting the animals.

References

[1] Bob Violino. *The history of RFID technology*. Jan. 2005.
URL: https://www.rfidjournal.com/the-history-of-rfid-technology.

[2] H. Stockman. *Communication by Means of Reflected Power*. In: Proceedings of the IRE 36.10 (1948), pp. 1196–1204. DOI: 10.1109/JRPROC.1948.226245.

[3] Diane Ward et al. *A Brief History of RFID*. 2009.
URL: http://www.u.arizona.edu/~obaca/rfid/history.html.

[4] Charles A. Walton. *Portable radio frequency emitting identifier*. U.S. Patent 4,384,288. May 1983.
URL: https://patents.google.com/patent/US4384288.

[5] K. Finkenzeller. *RFID Handbook*. John Wiley & Sons, 2010.

[6] ETSI. *EN 300 330: Short Range Devices (SRD); Radio equipment in the frequency range 9 kHz to 25 MHz and inductive loop systems in the frequency range 9 kHz to 30 MHz; Harmonised Standard covering the essential requirements of article 3.2 of the Directive 2014/53/EU*. May 2016.
URL: https://www.etsi.org/deliver/etsi_en/300300_300399/300330/02.01.01_60/en_300330v020101p.pdf.

[7] ETSI. *EN 302 208: Radio Frequency Identification Equipment operating in the band 865 MHz to 868 MHz with power levels up to 2 W and in the band 915 MHz to 921 MHz with power levels up to 4 W; Harmonised Standard for access to radio spectrum*. May 2020.
URL: https://www.etsi.org/deliver/etsi_en/302200_302299/302208/03.03.00_20/en_302208v030300a.pdf.

[8] ETSI. *EN 300 440: Short Range Devices (SRD); Radio equipment to be used in the 1 GHz to 40 GHz frequency range; Harmonised Standard covering the essential requirements of article 3.2 of Directive 2014/53/EU*. Mar. 2017.
URL: https://www.etsi.org/deliver/etsi_en/300400_300499/300440/02.01.01_60/en_300440v020101p.pdf.

[9] U.S. Department of Agriculture (USDA). *Animal disease traceability*. June 2020.
URL: https://www.aphis.usda.gov/aphis/ourfocus/animalhealth/SA_Traceability.

[10] Sarah Gough. *How RFID is transforming the livestock-management industry: RFID Journal Live!* Aug. 2021.
URL: https://rfidjournallive.com/content/blog/how-rfid-is-transforming-the-livestock-management-industry/.

[11] Texas Instruments. *TMS3705 datasheet*.
URL: https://www.ti.com/document-viewer/TMS3705/datasheet/device-overview-scbs881t6149#SCBS881t6149.

[12] Priority 1 Design. *FDX-B animal identification protocol description*.
URL: https://priority1design.com.au/fdx-b_animal_identification_protocol.html.

[13] Wikipedia contributors. *ISO 3166-1 — Wikipedia, The Free Encyclopedia*.
Online; accessed 31-March-2022.
URL: https://en.wikipedia.org/wiki/ISO_3166-1.

[14] Zhijiang Ni, Zhenjiang Gao and Hai Lin. *The Application of RFID in Automatic Feeding Machine for Single Daily Cow*. In: Deploying RFID . Ed. by Cristina Turcu. Rijeka: IntechOpen, 2011. Chap. 8. DOI: 10.5772/17608.
URL: https://doi.org/10.5772/17608.

[15] Priority 1 Design. *HDX Animal Identification protocol description*.
URL: https://priority1design.com.au/hdx_animal_identification_protocol.html.

[16] Langner Siegfried and Juergen Mayer. *TMS3705 Passive Antenna Solution*. Application note. July 2010.

[17] Pete Bevelacqua. *NFC antennas*.
URL: https://www.antenna-theory.com/definitions/nfc-antenna.php.

[18] Open Source Hardware Engineering. *Analysis and Design of Electrically Small Loop Antennas for LF and MF Applications - Version 4*. 2022.
URL: https://www.osengr.org/Articles/Loop-Antennas.pdf.

[19] Constantine A. Balanis. *Antenna theory: analysis and design*. John Wiley & Sons, 2016.

[20] Wikipedia contributors. *Ferrite (magnet) — Wikipedia, The Free Encyclopedia*.
Online; accessed 7-April-2022.
URL: https://en.wikipedia.org/wiki/Ferrite_(magnet)#Soft_ferrites.

[21] Wikipedia contributors. *Coercivity — Wikipedia, The Free Encyclopedia*.
Online; accessed 12-May-2022.
URL: https://en.wikipedia.org/wiki/Coercivity.

[22] Wikipedia contributors. *Permeability (electromagnetism) — Wikipedia, The Free Encyclopedia*.
Online; accessed 7-April-2022.
URL: https://en.wikipedia.org/wiki/Permeability_(electromagnetism).

[23] Open Source Hardware Engineering. *Inductance of Solenoids on Ferrite Rods - revision 2.0*. 2020.
URL: https://www.osengr.org/Articles/Ferrite-Rod-Inductance.pdf.

[24] Robert L. Boylestad. *Introductory circuit analysis*. Pearson Education, 2016.

[25] Wikipedia contributors. *Q factor — Wikipedia, The Free Encyclopedia*.
Online; accessed 28-May-2022.
URL: https://en.wikipedia.org/wiki/Q_factor.

[26] Wikipedia contributors. *Antenna factor — Wikipedia, The Free Encyclopedia*.
Online; accessed 6-June-2022.
URL: https://en.wikipedia.org/wiki/Antenna_factor.

[27] SIDEN-TELEC. *NOTICE D'UTILISATION CADRE Réf: CT1, H-FIELD 10 - 150 kHz*. Application note. June 1979.

[28] EM Microelectronic. *EM4095 Booster Circuit, Application Note*.
URL: https://docplayer.net/storage/65/53099730/1653727858/SqRzqFYK1g7nowbzzn5ojQ/53099730.pdf.

[29] Texas Instruments. *TMS3705 Range Extender Power Solution Using UCC27424-Q1*.
URL: https://www.ti.com/lit/an/scba031/scba031.pdf.

[30] Fair Rite Corp. *78 Material Data Sheet*.
URL: https://www.fair-rite.com/78-material-data-sheet/.

Appendix A EM4095 Basestation Schematic

A.1 Main Schematic

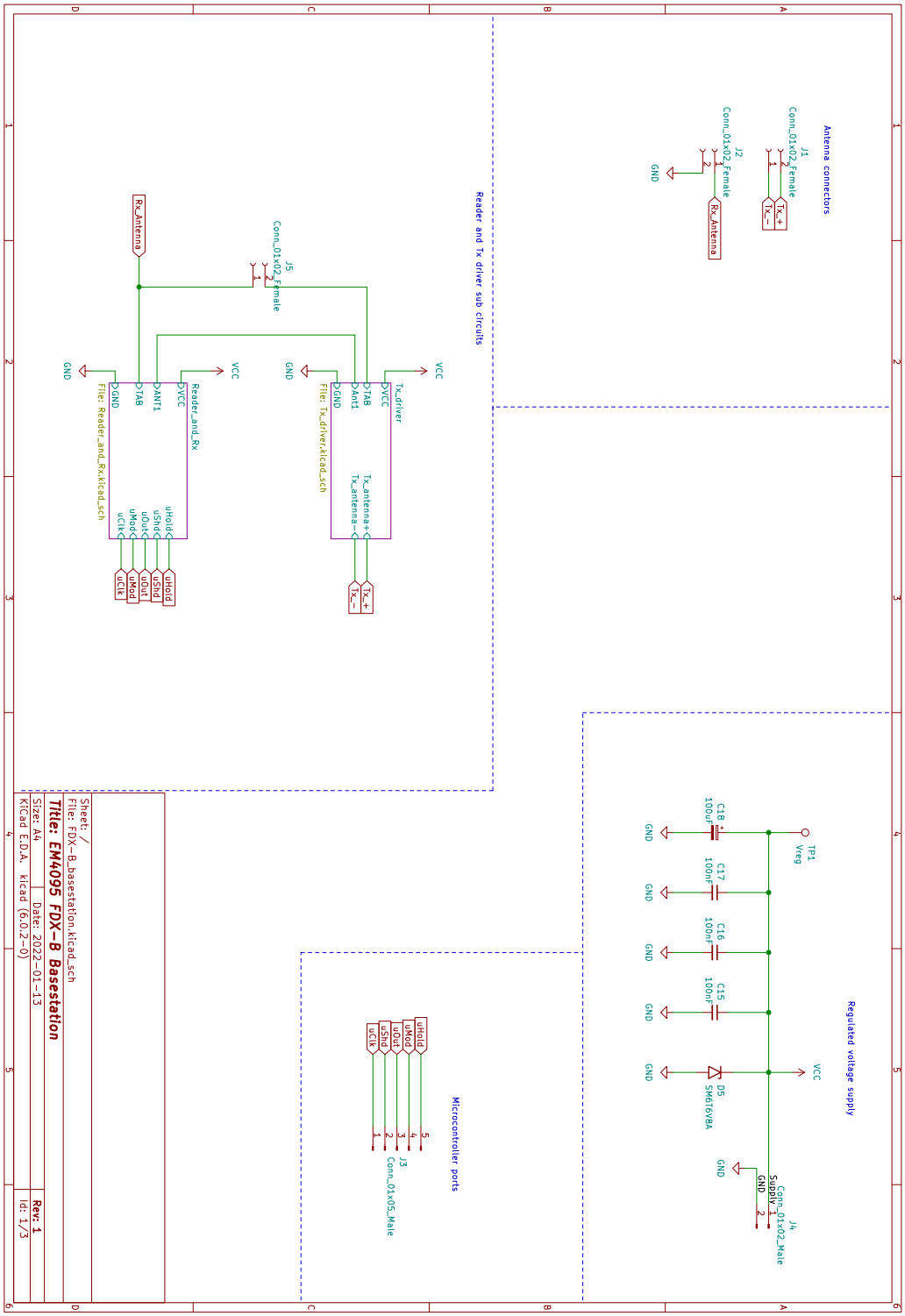

A.2 Driver Schematic

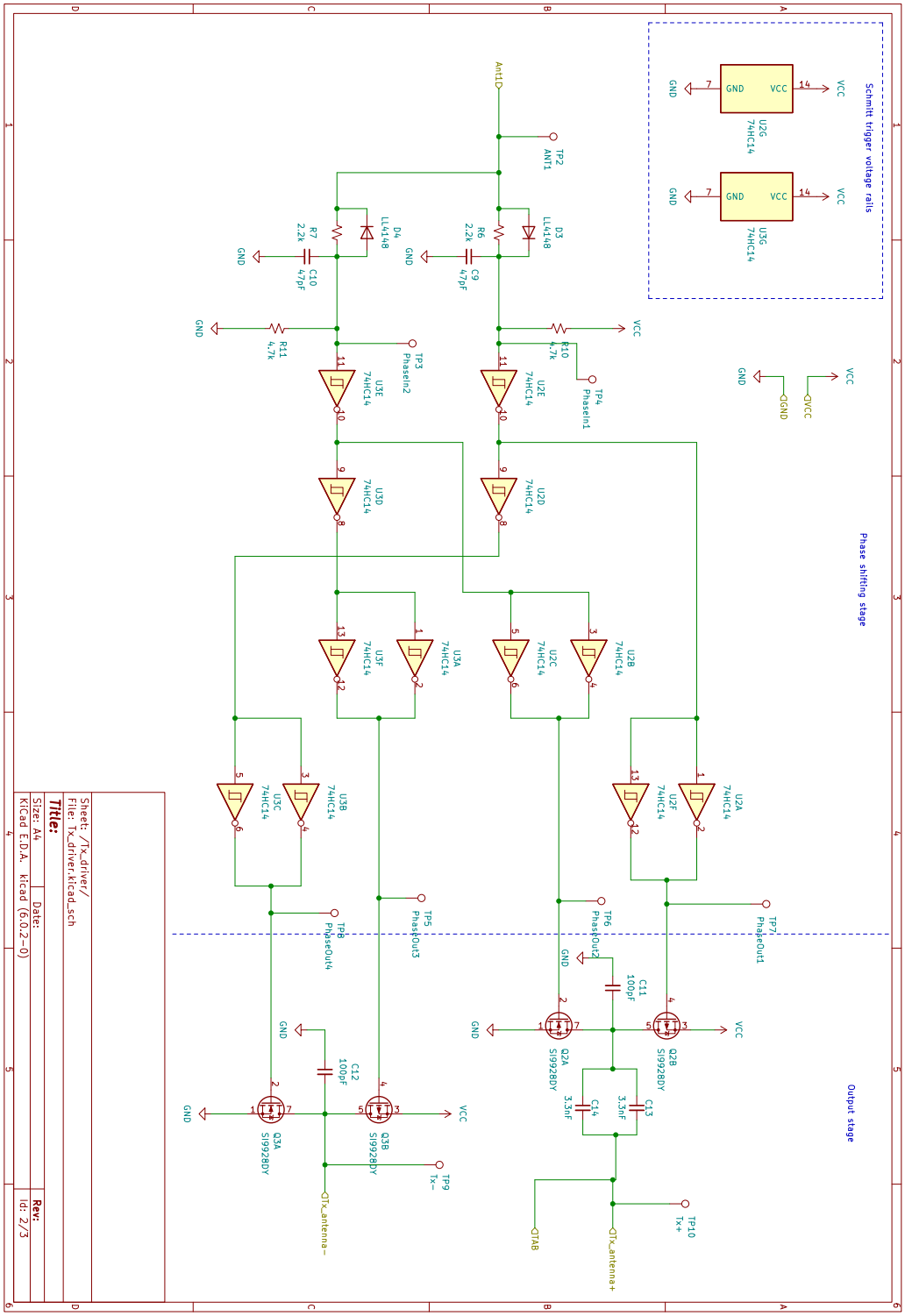

A.3 Demodulator Schematic

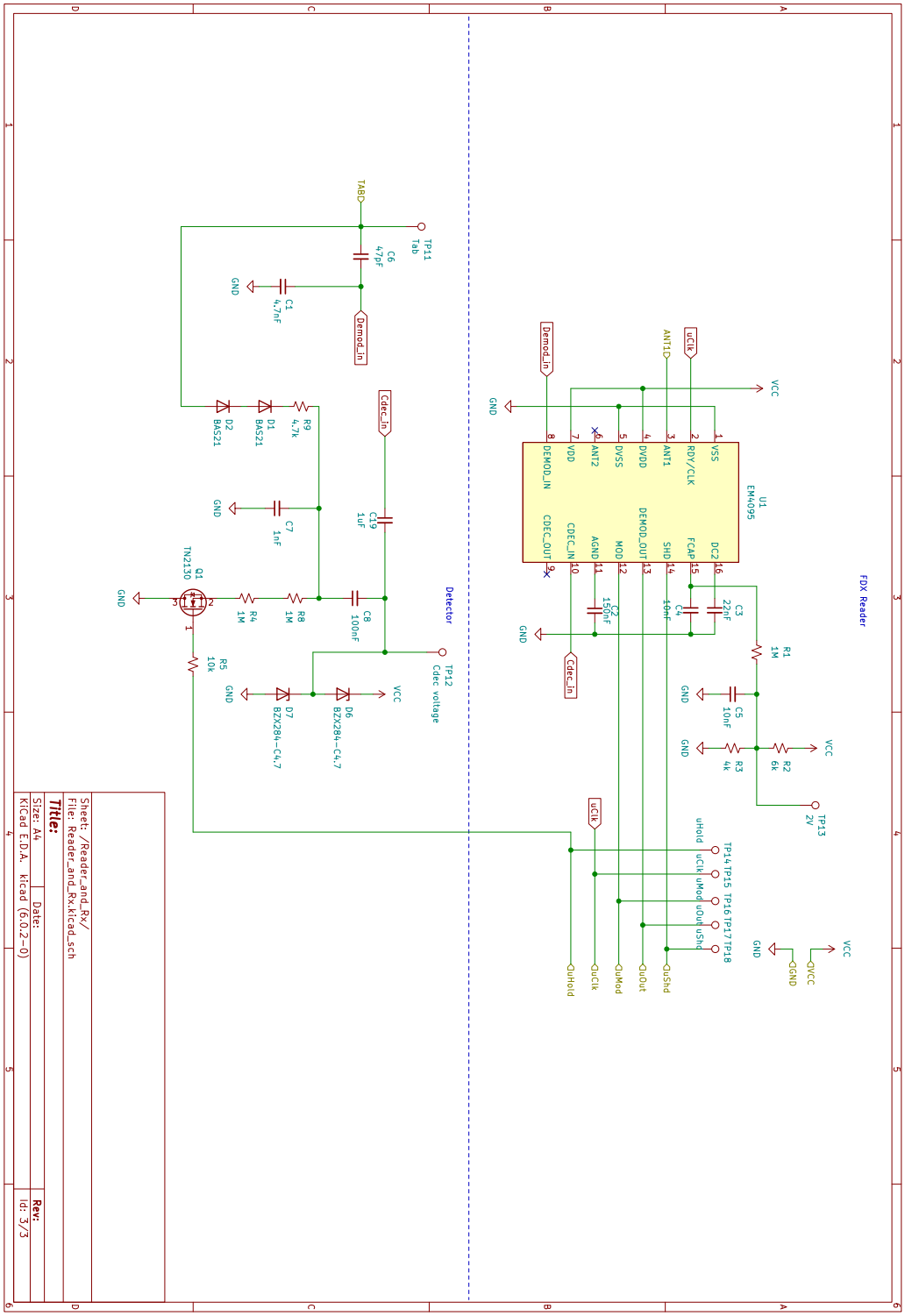

Appendix B EM4095 Basestation Layout

B.1 Top Layer

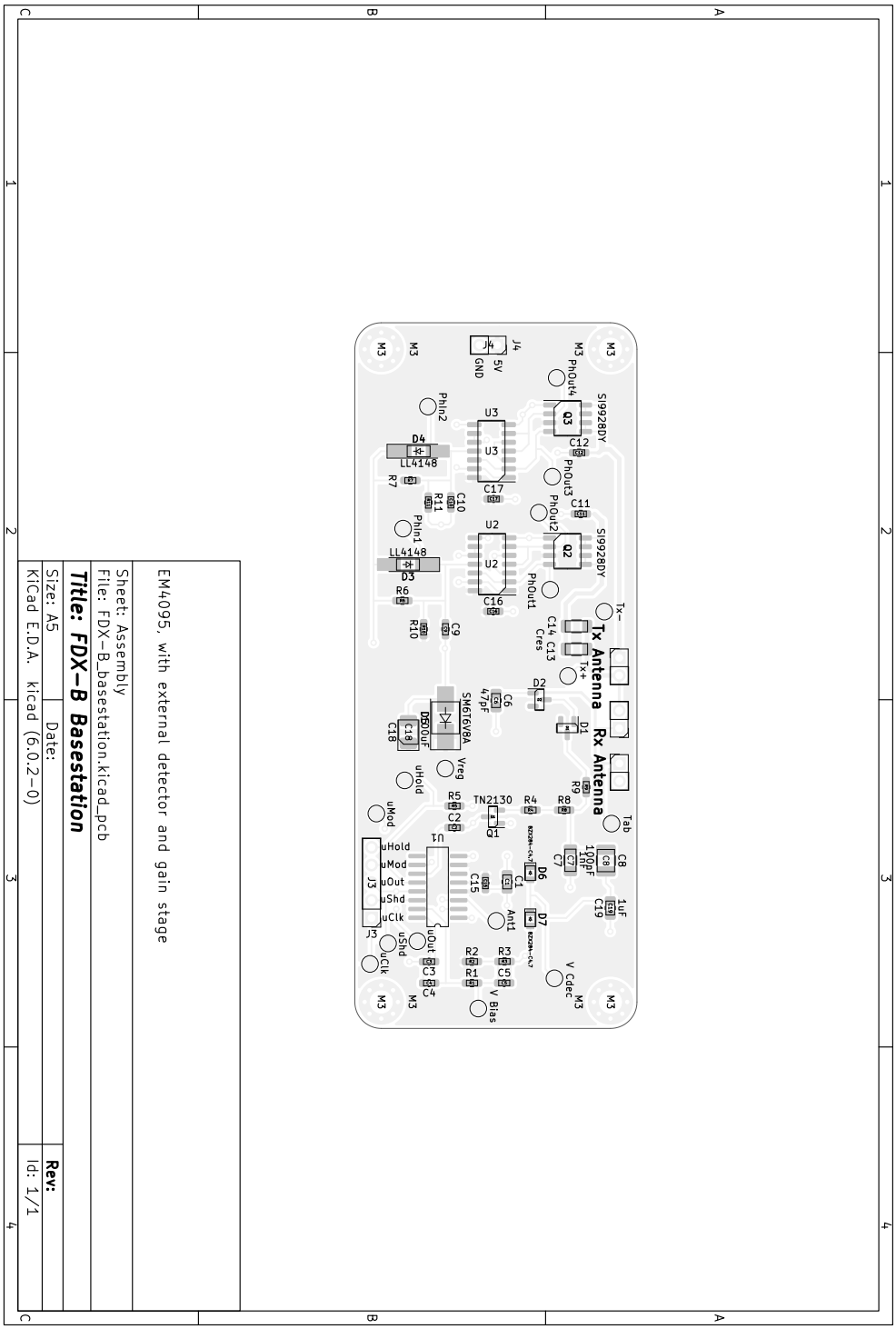

B.2 Bottom Layer

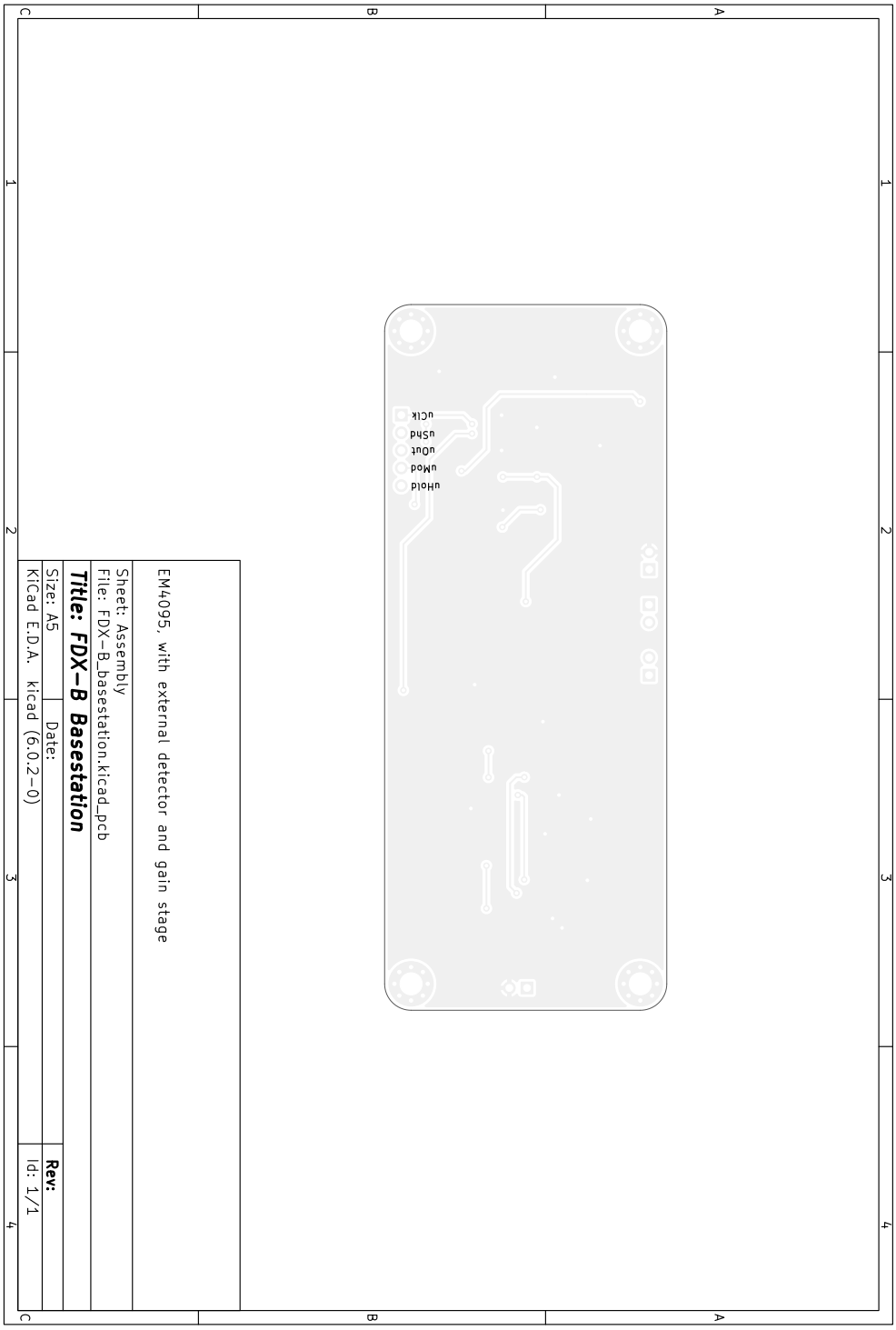

Appendix C Source code for interfacing EM4095 with ATmega328P

```
/*
*   +-------------------------------------------------------------------+
*   |   C source for connecting EM4095 with ATmega328P for reading      |
*   |                FDX-B ISO11784/5 animal RFID tags.                 |
*   |                                                                   |
*   |                                                                   |
*   |                                                                   |
*   |                                                                   |
*   +-------------------------------------------------------------------+
*/

//=========================== Includes ======================
#include "led.h"
#include "usart.h"
#include <stdbool.h>
#include <avr/io.h>
#include <avr/interrupt.h>


//=========================== Global variables ======================
volatile int isrcnt = 0;
volatile int current;
volatile bool flag = false;
volatile char data;


//=========================== Delay routine ======================
void delay() {
  for (volatile int i = 0; i < 1000; i++) {
    for (volatile int j = 0; j < 1000; j++) {
    }
  }
}


//=========================== Interrupt routine ======================
ISR(TIMER1_CAPT_vect){
  current = ICR1;
  TCNT1 = 0;
  isrcnt++;
}

//=========================Decode routine ======================

char* decode(int time){
  //char symbol[2];
  char* symbol;
  if ((4400 > time) && (time > 3400)) {
    symbol="0";
  }
  else if ((6400 > time) && (time > 5400) && (flag == false)){
    flag = true;
    symbol="1";
```

```
  }
  else if ((6400 > time) && (time > 5400) && (flag == true)){
    flag = false;
    symbol = "01";
  }
  else if((8000 > time) && (time > 7000)){
    symbol = "11";
  }
  else{
    symbol = "Error";
  }
  return symbol;
}

//========================== Main routine =======================
int main () {
  cli();
  TCCR1A = 0;           // Set all bits in TCCR1A register to zero, to enable
  ↪  timer1
  TCCR1B = 0;           // Set all bits in TCCR1B register to zero, to enable
  ↪  timer1
  TCCR1B = 0b11000001;  // Enable noise cancler, trigger on rising edge, no
  ↪  prescaler
  TIMSK1 = 0b00100000;  // Enable input capture



  /* initialize usart */
  usart_init();

  char icrval[16];

  /* initialize LED */
  init_led();
  sei();

  while(1) {

    char* decoded_symbols;
    decoded_symbols = decode(current);
    usart_print(decoded_symbols);




    //led_toggle();


  }

  return 0;
}
```

Appendix D TMS3705 Basestation Schematic

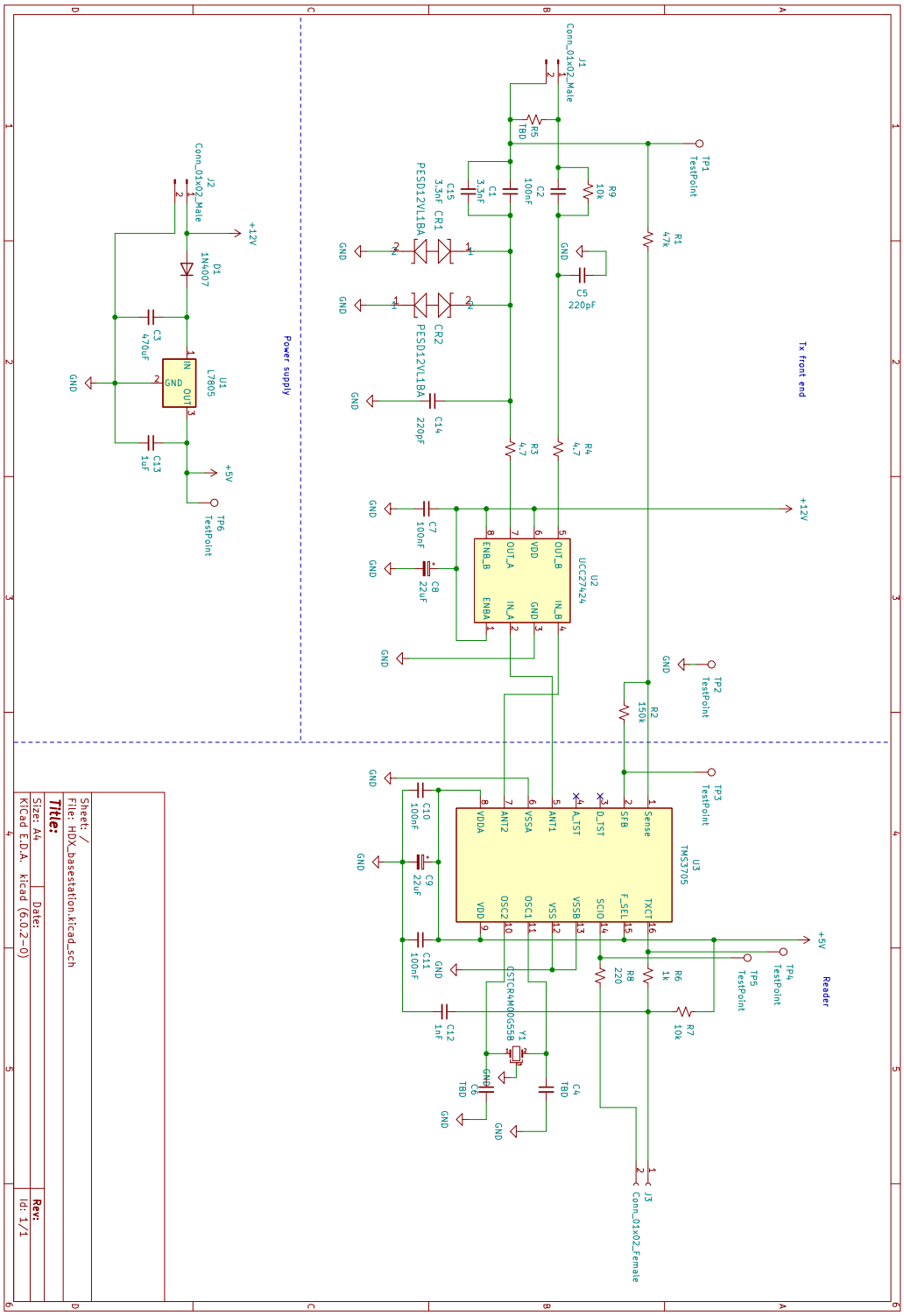

Appendix E TMS3705 Basestation Layout

E.1 Top Layer

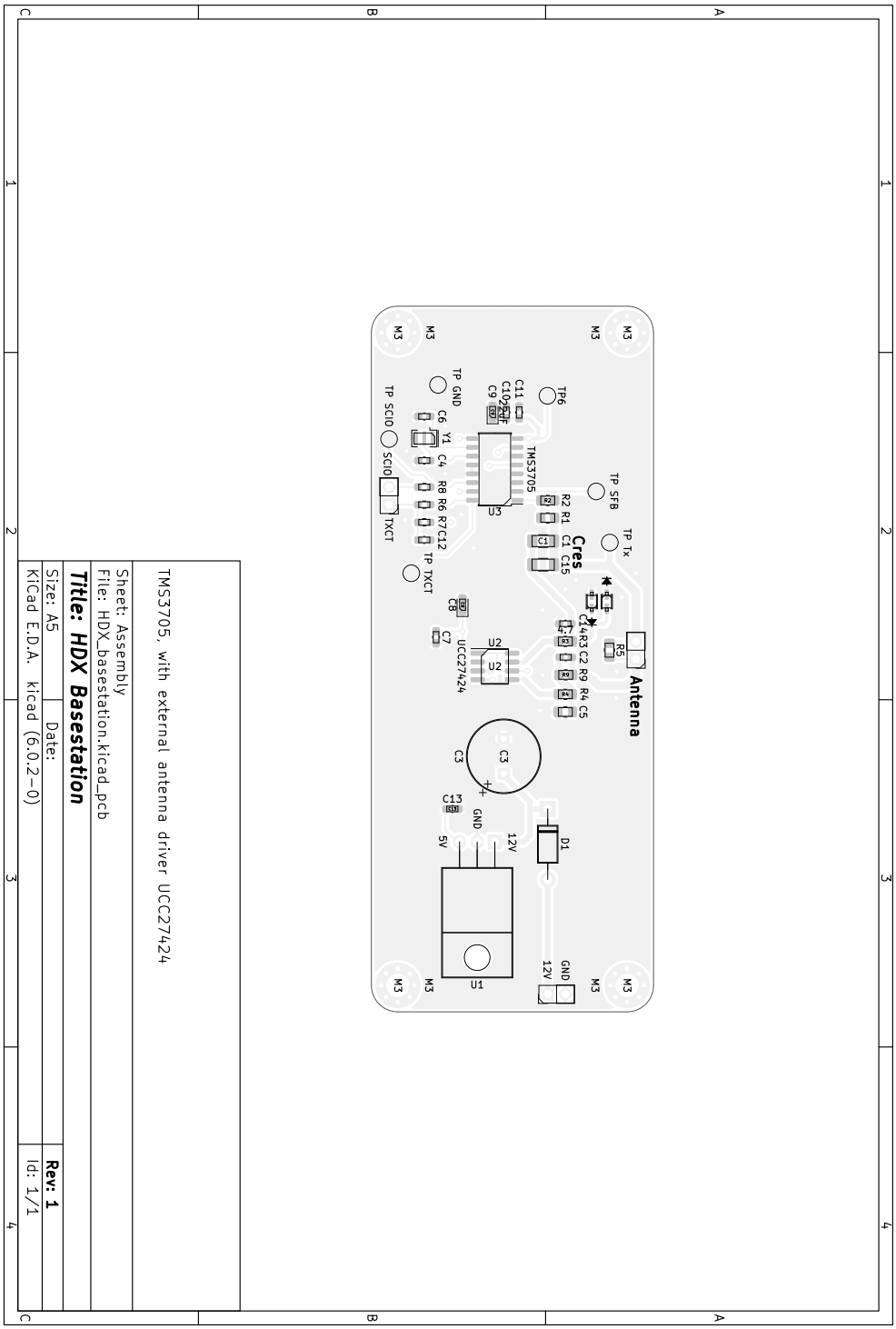

E.2 Bottom Layer

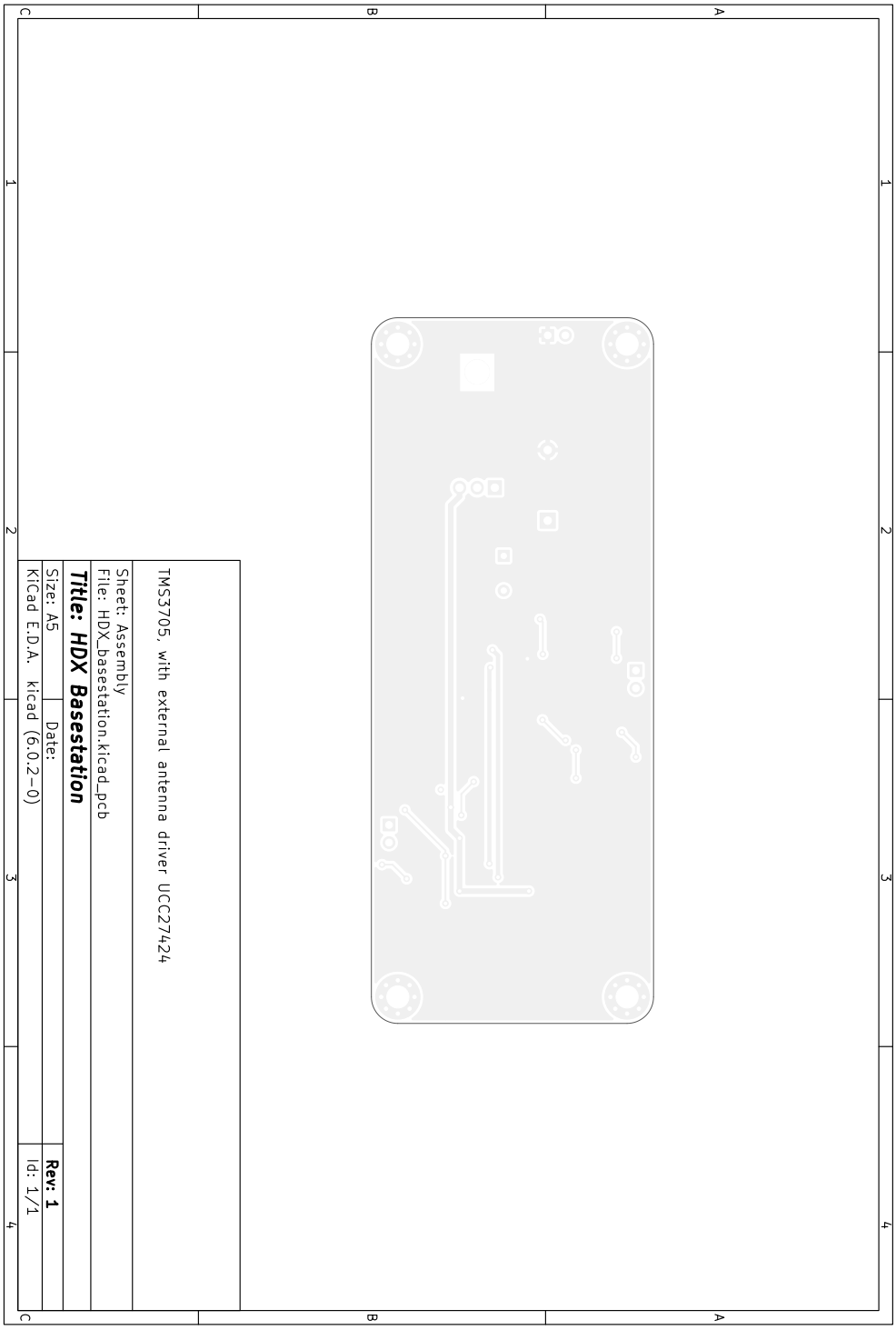

Appendix F Source code for interfacing TMS3705 with ATmega328P

```
/*
*   +-------------------------------------------------------------------+
*   |   C source for interfacing TMS3705 with ATmega328P for            |
*   |      Reading HDX ISO11784/5 based animal RFID tags.               |
*   |                                                                   |
*   |                                                                   |
*   |                                                                   |
*   |                                                                   |
*   +-------------------------------------------------------------------+
*/

//============================== Includes ==============================
#include "led.h"
#include "usart.h"
#include <stdbool.h>
#include <avr/io.h>
#include <avr/interrupt.h>


//========================== Global variables ==========================
volatile int temp2 = 0;
volatile int current[255];
volatile bool flag = false;
volatile char data;


//============================ Delay routine ============================
void delay() {
  for (volatile int i = 0; i < 1000; i++) {
    for (volatile int j = 0; j < 1000; j++) {
    }
  }
}


//=================== External Interrupt routine ====================
ISR(INT1_vect){
  EIMSK = 0b00000000;     //External interrupt on INT1 disable
  EICRA = 0b00000000;     //External interrupt on INT1 disable

  //------Enable CTC interrupt for sampling SCIO pin-----------

  TCCR0A = 0b00000000;    //Set all bits in TimerCounter0 to zero
  TCCR0B = 0b00000010;    //Set CS01 to 1 => prescaler = 8, tick @ 500ns

  TIMSK0 = 0b00000010;    //Enables compare match for timer0
  OCR0A = 128;            //Set top value to 128 => compare @ each 64us

}

//==================== CTC Interrupt routine ====================
ISR(TIMER0_COMPA_vect){
  TCNT0 =  0;                           //reset timer
```

```
  read = (PIND >> 3 & 0b00001000 >> 3); //check pins value


}


//================================ Main routine ================================
int main () {
  cli();
  EIMSK = 0b00000010;    // External interrupt Request 1 enable
  EICRA = 0b00001100;    // External interrupt for rising edge on INT1 (D3 pin)
  EIFR = 0b00000000;     // External interrupt flag bit 1 gets set when interrupt
  ↪  occurs

  /* initialize usart */
  usart_init();

  char icrval[16];

  /* initialize LED */
  init_led();
  sei();

  while(1) {


    if (temp2 >= 245){
      for(int i = 0; i>245; i++){
        decode(current[i]);
      }
      for(int i = 0; i>sizeof(data)/sizeof(data[0]) - 1; i++){
        char icrval[16];
        itoa(data, icrval, 10);
        usart_set_message(data);
        //led_toggle();
        usart_print(icrval);

      }

    }



    //delay();

  }

  return 0;
}
```

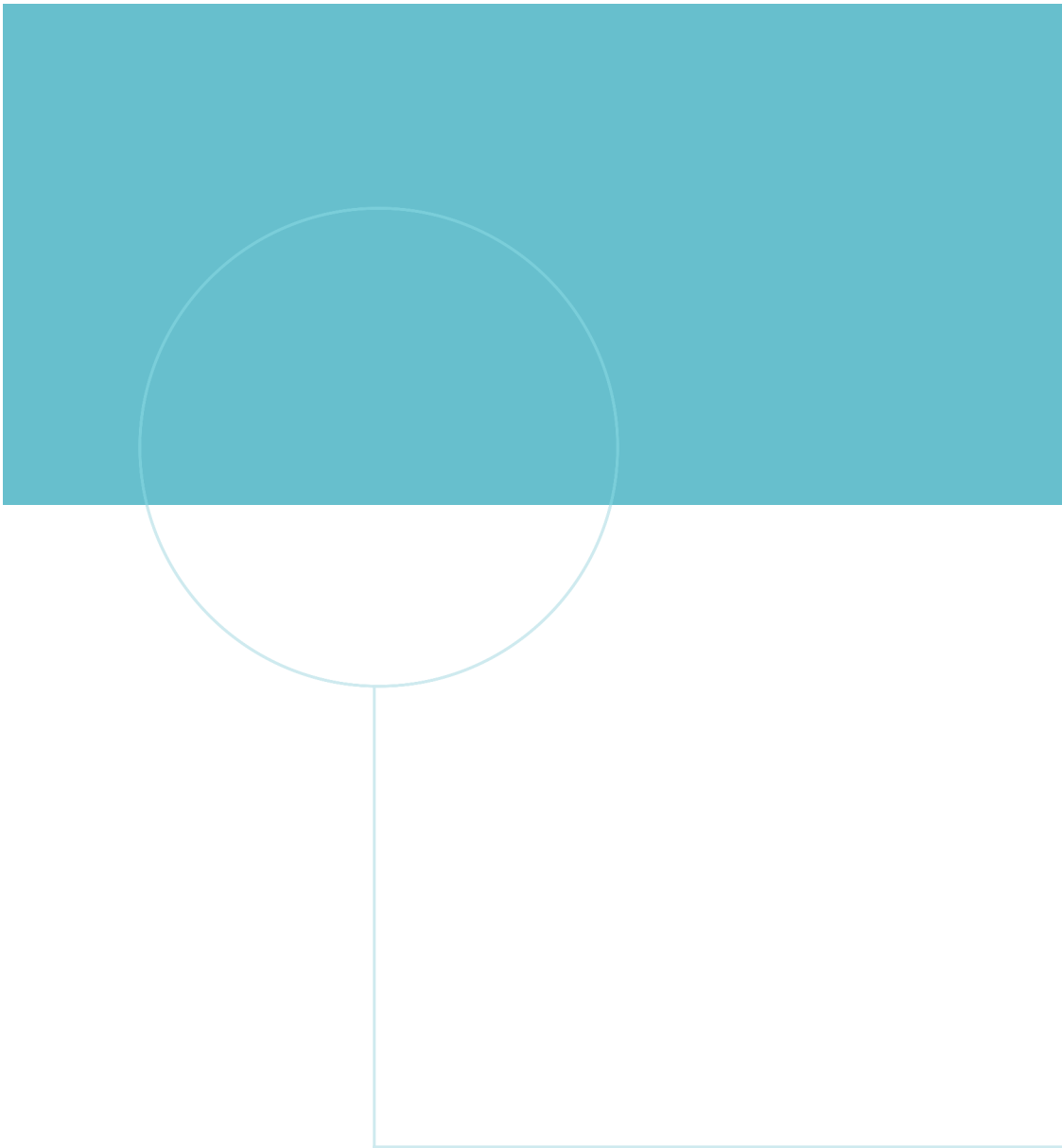

NTNU

Norwegian University of
Science and Technology